



**OFFSHORE TECHNOLOGY
RESEARCH CENTER**

Hybrid Wave Model and Its Applications

By

Jun Yang

AB

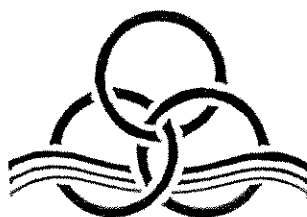
24B

Hybrid Wave Model and Its Applications

By

Jun Yang

NSF# CDR-8721512



OFFSHORE
TECHNOLOGY
RESEARCH
CENTER

A National Science Foundation Engineering Research Center

3/99A9975

For more information contact:

Offshore Technology Research Center
Texas A&M University
1200 Mariner Drive
College Station, TX 77845-3400
(409) 845-6000

or,

Center for Offshore Technology
The University of Texas at Austin
Department of Civil Engineering
ECJ 4.200
Austin, Texas 78712
(512) 471-3753

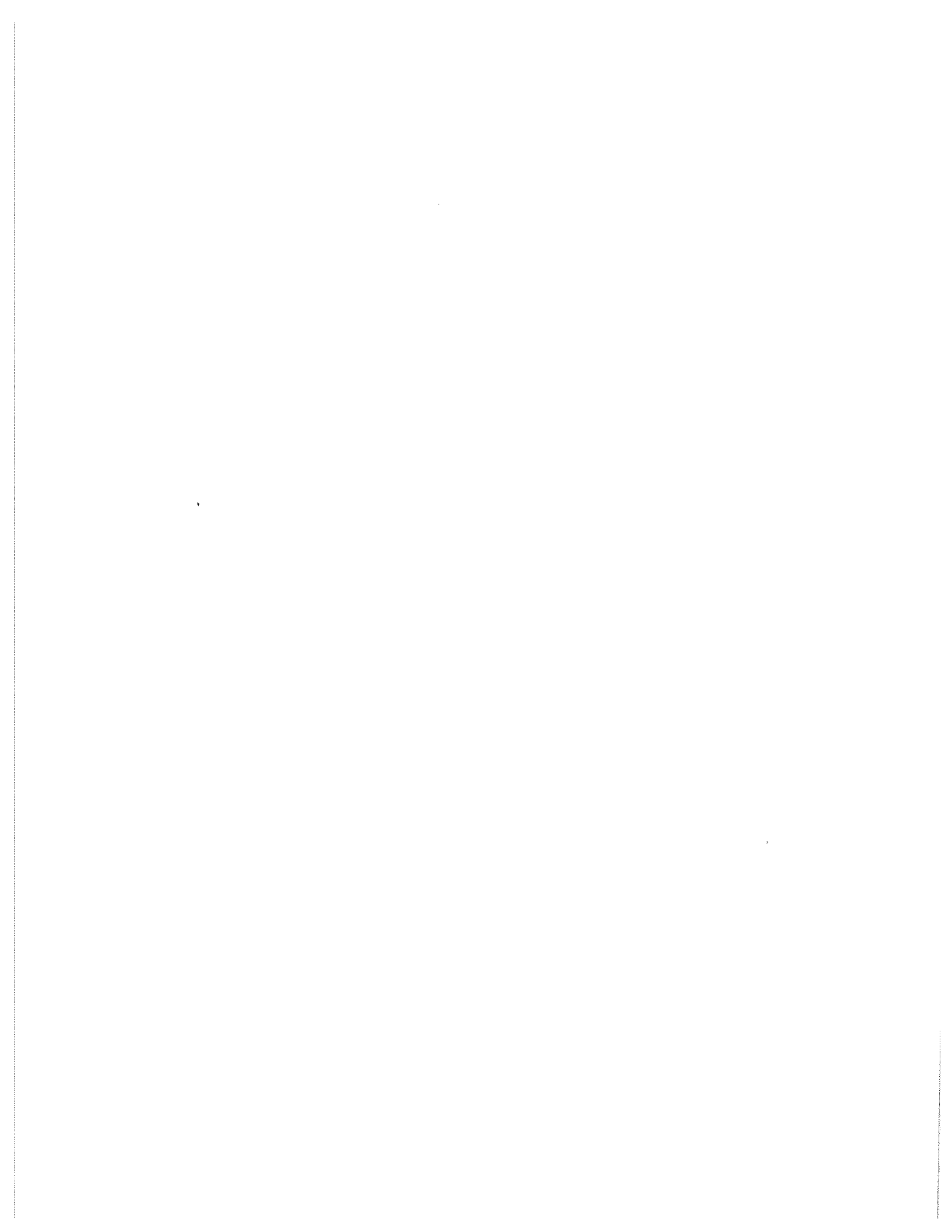
LIST OF TABLES

TABLE		Page
I	Interactions between four wave bands: P: phase modulation method (PMM); M: mode-coupling method (MCM).	25
II	Zeroth moments of a Gamma spectrum with $5\omega_p-9\omega_p$ cutoff frequency, nominal steepness $s=0.055$	42
III	Surface elevation at $t=54.5$ s of a Gamma spectrum with $5\omega_p-9\omega_p$ cutoff frequency, nominal steepness $s=0.055$	44
IV	Significant wave height against nominal spectral steepness s	52

LIST OF FIGURES

FIGURE	Page
1	Band division of directional hybrid wave model. 25
2	Resultant horizontal velocity in x -direction of a long wave and a short wave obtained by the PMM ($-●-$), ($- - -$) is the leading order solution of short wave velocity by the MCM, long wave velocity is ($—$) for reference, the velocity is nondimensionalized by $(k_l/g)^{0.5}$. . . 31
3	Comparison between the MCM ($—$) and the PMM ($- - -$) for a dual free-wave spectrum with $\varepsilon_1 = 0.10$, $\varepsilon_l = 0.3822$: (a) surface elevation; (b) horizontal velocity in x direction; (c) vertical acceleration. 33
4	Comparison between MCM ($- - -$) and PMM ($-●-$) for a dual free-wave spectrum with $\varepsilon_1 = 0.20$, $\varepsilon_l = 0.139$, x -direction horizontal velocity profiles of the long and short waves up to the leading order (I $—$) and the second order (II $—$), and the long-wave velocity only ($- x -$) 35
5	Same as Figure 4 except the short wave is 180 degree out of phase of the long-wave component. 37
6	Truncated Gamma spectra, ($—$): $p=5$, ($- - -$): $p=9$, nominal steepness $s=0.06$ 39
7	Band division of a wide wave spectrum. 41
8	Horizontal velocity profile against cutoff frequency by the MCM, nominal steepness $s=0.055$ 43
9	Horizontal velocity profile against cutoff frequency by the PMM, same spectrum as Figure 8. 45
10	Free-wave components consisting of an unidirectional irregular wave trains: (a) amplitudes, (b) initial phases. 46

FIGURE	Page
11	Time series of (a) surface elevation (b) horizontal velocity (c) horizontal velocity at location of (10.00,-8.25)m downstream, by DHWM (—) and UHWM (- - -). 47
12	Definition sketch of a fix-bottom structure. 50
13	μ_1 versus s , (a) drag force (b) inertia force; (-o-): Gamma spectrum with $p=9$; (- Δ -): Gamma Spectrum with $p=5$, $\omega_c = 5\omega_p$ 54
14	μ_2 versus s , (a) drag force (b) inertia force; (-o-): Gamma spectrum with $p=9$; (- Δ -): Gamma Spectrum with $p=5$, $\omega_c = 5\omega_p$ 55
15	Water particle velocity and acceleration in a periodic wave 56
16	μ_3 versus s , (a) drag force (b) inertia force; (-o-): Gamma spectrum with $p=9$; (- Δ -): Gamma Spectrum with $p=5$, $\omega_c = 5\omega_p$ 57
17	μ_c versus s , (a) drag force (b) inertia force; (-o-): HWM; (- Δ -): MCM. 60
18	μ_w versus s , (a) drag force (b) inertia force; (-o-): Gamma spectrum with $p=9$; (- Δ -): Gamma Spectrum with $p=5$, $\omega_c = 5\omega_p$ 63



CHAPTER I

INTRODUCTION

A. Background

The initial substantive interest in and contributions to water wave mechanics can be traced back to more than a century ago, beginning with the analysis of linear wave theory by Airy in 1845. One of the main purposes of studying ocean waves is to understand the interaction between waves and ocean structures, which are commonly found in a variety of offshore, coastal, naval architecture, oceanographic and environmental applications. For instance, to compute the waves loads on a slender offshore structure using the Morison equation (Morison et al. 1950), one needs to know the wave kinematics.

$$\mathbf{f} = \frac{1}{2}C_D\rho D|\mathbf{U} - \mathbf{U}_b|(\mathbf{U} - \mathbf{U}_b)ds + C_M\rho A(\dot{\mathbf{U}} - \dot{\mathbf{U}}_b)ds. \quad (1.1)$$

For bigger size offshore structures, finite element methods (FEM) are usually applied to compute the wave forces, which are numerical integrals of the wave pressure on the elements. The pressure is computed by the Bernoulli equation

$$\frac{\partial\Phi}{\partial t} + \frac{1}{2}|\nabla\Phi|^2 + g\eta = C_0, \quad (1.2)$$

which also requires the computation of the wave kinematics.

For regular waves, or periodic waves, the prediction of wave kinematics by the fifth order *Stokes* wave theory or Dean's *Stream Function* (1972) is satisfactory. However it is not by simple superposition of the individual waves that we can obtain the wave kinematics of irregular waves. It is known that linear wave theory may over

The journal model is *Journal of Fluid Mechanics*.

predict the wave kinematics above the still water level (swl) under irregular ocean waves. Based on linear wave theory, a range of empirical approximations have been proposed to tune the near surface wave kinematics. But these approximations lack theoretical grounds and may either under predict or over predict wave kinematics under irregular ocean waves (Donelan et al. 1992).

The second order conventional perturbation solution, or called mode-coupling method (MCM) (Longuet-Higgins 1962) is an improvement to linear and modified linear wave theories. However, the conventional perturbation approach was developed for narrow-band wave interactions. It may be divergent when the wavelengths of the two interacting wave components are quite different (Zhang et al. 1993). The phase modulation method (PMM) is a complementary solution to the divergence of the MCM (Zhang et al. 1993). It directly describes the modulation of short wave components by long wave components. A new nonlinear wave model, called the hybrid wave model (HWM), employs both MCM and PMM to model the wave-wave interactions of ocean waves. The HWM divides the spectrum into several wave bands and computes the interactions of close-frequency wave components within the same and neighboring wave bands by the MCM and interactions of relatively far-apart wave components by the PMM. The unidirectional HWM proposed by Zhang et al. (1996) was recently extended to allow directionality of ocean waves. The derivation of the directional hybrid wave model (DHWM) using a multi-parameter perturbation technique is detailed in this research.

Based on the precise knowledge of wave kinematics provided by the HWM, wave forces on slender offshore structures using the Morison Equation are computed. The effects of surface fluctuation and wave nonlinearity are further investigated with the HWM. Hu et al. (1995) applied the second-order MCM to study the surface fluctuation and wave nonlinear effects on single degree of freedom (SDOF) structures.

They found dramatic changes of near surface kinematics and wave forces at different cutoff frequencies. They argued that the changes were caused by the contribution of the leading order short wave components. However, their arguments are incorrect because the second-order MCM is divergent to compute the nonlinear wave-wave interactions of a broad wave spectrum and hence the kinematics related wave forces diverge as well.

B. Literature Review

The solution for two unidirectional wave components with close frequencies using the MCM was obtained by Longuet-Higgins (1962). The second-order solution was obtained using a perturbation approach and satisfied the nonlinear boundary conditions by Taylor's expansion at the swl. Zhang et al. (1993) proved that when the wavelength ratio of short to long wave, ε_l becomes smaller than the long wave steepness, the truncated solution of the MCM becomes divergent.

In contrast to the MCM, which describes the effects of wave-wave interaction in terms of high order solutions, the PMM considers the consequence of the interaction as the modulation of the short-wave component. The introduction of the PMM overcame the divergence problem of the MCM for interactions between long and short wave that are of quite different wave lengths. Based on the unidirectional MCM and PMM, the unidirectional HWM (UHWM) was developed (Zhang et al. 1996). For spectral ocean waves, it divides the spectrum into several wave bands and model the wave-wave interaction between free-wave components by the MCM and PMM, correspondingly: i.e. interactions of close frequency free-wave components by the MCM and those of free-wave components relatively far-apart by the PMM.

The UHWM was applied in the research of unidirectional irregular wave decom-

position and prediction (Zhang et al. 1996). Excellent agreements have been found between the prediction of the UHWM and experiment results (Spell et al. 1996). The HWM was later developed to a directional wave model by using a multi-parameter perturbation approach (Zhang et al. 1998). The DHWM is capable of computing nonlinear wave-wave interaction of short-crested ocean waves and has been applied in the research of deterministic decomposition and prediction of directional irregular ocean waves (Zhang et al. 1998).

The prediction of wave kinematics under irregular waves has been the focus of ocean wave research for many years. A range of prediction methods and theories have been proposed. Besides the MCM, many empirical stretching and extrapolation methods have been proposed based on linear wave theory. Wheeler (1969) proposed a stretching method that has been recommended for offshore engineering practice (API 1993). But Wheeler stretching may under predict the kinematics above the swl (Donelan et al. 1992). Laboratory and field data has shown that these coordinate stretching methods may either consistently under predict or over predict the wave kinematics above swl(Donelan et al. 1992; Zhang et al. 1996). The predictive potential and comparative performance of these methods need more detailed evaluation (Sobey 1990).

Wave forces on slender structures are usually computed using the Morison equation because the diffraction effect of the structures is negligible (Sarpkaya 1981). Accurate estimation of the wave forces computed by the Morison equation requires precise knowledge of the wave kinematics. For relatively strong nonlinear waves, nonlinear wave models are usually applied to obtain more accurate wave kinematics. Total wave forces are the integrations of the segmental wave forces along the structure. The consideration of the fluctuating surface elevation, which is referred to as the wave intermittency, is also important in the computation of the wave forces. Tung

et al. (1991) studied the effects of free surface fluctuation on structure wave loads. It was concluded that for sinusoidal waves the free surface fluctuation has important effects on wave fields and force especially in the vicinity of the swl. Hu et al. (1995) applied the MCM to study the effects of surface fluctuation and wave nonlinearity on wave loads under irregular wave conditions. It was concluded that the effects were both crucial under relatively steep waves and neglecting either of them will *severely* underestimate the wave forces on the structure. It was also found that the prediction of wave forces was very sensitive to the cutoff frequency of the spectrum and the inclusion of high frequency wave components greatly increased the wave loads under steep wave conditions. However, it is the divergence of the MCM that caused the sensitivity to the cutoff frequency and exaggerated the effects of wave nonlinearity and intermittency on wave forces. Using the HWM, we investigated the effects of surface intermittency and wave nonlinearity on SDOF structure wave loads under irregular wave conditions. Important conclusions of the nonlinear effects on the wave forces are given based on analysis and the numerical results. The determination of the cutoff frequency in the design practice is also discussed.

API (1993) proposed Wheeler stretching method to compute wave forces on slender bodies under irregular ocean waves. In this thesis, we will compare the prediction of wave forces on SDOF structures by the HWM and the API approach under strong nonlinear waves. Important conclusions based on the comparison are given.

C. Objectives

Main objective of this research is to introduce the DHWM and its applications in the aspect of ocean engineering. Specific objectives include

- (1) To introduce the HWM. The HWM includes both of the MCM and PMM,

which are derived by a single- and multi-parameter perturbation technique respectively.

(2) To apply the HWM to predict the wave kinematics under irregular oceans and compare the predictions by the MCM and PMM.

(3) To compute wave forces on SDOF structures using the Morison equation based on the HWM. To investigate the effects of surface intermittency and wave nonlinearity on wave loads and compare the predictions between linear and linear stretching methods. Give important conclusions of the nonlinear effects on wave forces. Propose a cutoff frequency in the offshore design practice.

CHAPTER II

HYBRID WAVE MODEL

For an incompressible and irrotational free surface flow, the governing equation and boundary conditions can be written as

$$\nabla^2 \Phi = 0, \quad -h \leq z \leq \eta \quad (2.1)$$

$$\frac{\partial \Phi}{\partial t} + \frac{1}{2} |\nabla \Phi|^2 + g\eta = C_0, \quad \text{at } z = \eta \quad (2.2)$$

$$\frac{\partial \eta}{\partial t} + \frac{\partial \Phi}{\partial x} \frac{\partial \eta}{\partial x} + \frac{\partial \Phi}{\partial y} \frac{\partial \eta}{\partial y} = \frac{\partial \Phi}{\partial z}, \quad \text{at } z = \eta, \quad (2.3)$$

$$\frac{\partial \Phi}{\partial z} = 0, \quad \text{at } z = -h, \quad (2.4)$$

where Φ is the velocity potential, η the surface elevation, t time, g the gravitational acceleration and h the water depth which is assumed to be uniform in this study. The x -axis is set at the calm water level, the y -axis is orthogonal to the x -axis in the horizontal plane, and the z -axis is pointing upwards. C_0 is the Bernoulli constant which will be chosen to ensure that $z = 0$ is located at the still water level.

The conventional mode coupling method (MCM) (Longuet-Higgins 1962) may render the truncated solutions for the wave-wave interaction problem in the order of wave steepness, defined as the product of the wave number and amplitude. When the ratio of the short-wavelength to that of the long wave, ε_l , is of $O(1)$, the MCM converges very quickly. However, when ε_l is small and approaches the long-wave steepness ε_1 , the truncated solution converges slowly and eventually diverges (Zhang et al. 1993).

The phase modulation method (PMM) proposed by Zhang et al. (1993) is a complementary solution to the the MCM. It considers the consequence of wave interactions as the modulation of the short wave and describes it directly in the solution for

the short-wave component. The PMM has been proven to be identical to the MCM approach when $\varepsilon_1 \ll \varepsilon_l < 0.5$. However, as ε_1 gets bigger and eventually greater than ε_l , the MCM solution diverges, while the PMM is convergent. But, when $\varepsilon_l > 0.5$, the PMM can not accurately predict the slowly varying interaction between the two wave components at third order in wave steepness (Zhang et al. 1993).

The HWM combines the MCM with the PMM to solve for the wave-wave interactions of broad-band spectral waves. The model employs the MCM for interactions between wave components, which are close in the frequency domain and the PMM for short-long waves that are relatively far apart in the frequency domain.

A. Mode Coupling Method

Longuet-Higgins (1962) gave a typical conventional perturbation solution and derived the solution up to second order in wave steepness. A third order approximation for two deep water short crested waves using the same approach was later given by Hsu (1979). The solution of the velocity potential of the interaction between two directional waves of intermediate water depth can be obtained using the same approach.

The potential function and surface elevation are expanded as

$$\Phi = \Phi^{(1)} + \varepsilon\Phi^{(2)} + \varepsilon^2\Phi^{(3)} + \dots, \quad (2.5a)$$

$$\eta = \eta^{(1)} + \varepsilon\eta^{(2)} + \varepsilon^2\eta^{(3)} + \dots, \quad (2.5b)$$

where ε is the wave steepness.

Substituting Equation (2.5a) and (2.5b) into Equations (2.1) – (2.4), the following leading order equations are obtained.

$$\nabla^2\Phi^{(1)} = 0, \quad (2.6)$$

$$\frac{\partial \Phi^{(1)}}{\partial t} + g\eta^{(1)} = 0, \quad \text{at } z = 0, \quad (2.7)$$

$$\frac{\partial \eta^{(1)}}{\partial t} - \frac{\partial \Phi^{(1)}}{\partial z} = 0, \quad \text{at } z = 0, \quad (2.8)$$

$$\frac{\partial \Phi^{(1)}}{\partial z} = 0, \quad \text{at } z = -h. \quad (2.9)$$

Eliminating $\eta^{(1)}$ from Equation (2.7), (2.8) gives

$$\frac{\partial^2 \Phi^{(1)}}{\partial t^2} + g \frac{\partial \Phi^{(1)}}{\partial z} = 0, \quad \text{at } z = 0. \quad (2.10)$$

As a solution for these equations, we select the first-order solution corresponding to two progressive directional surface waves of wave-number vector \mathbf{k}_1 and \mathbf{k}_2 .

$$\Phi^{(1)} = \frac{a_1 g \cosh[k_1(z+h)]}{\omega_1 \cosh(k_1 h)} \sin \theta_1 + \frac{a_2 g \cosh[k_2(z+h)]}{\omega_2 \cosh(k_2 h)} \sin \theta_2, \quad (2.11)$$

where for short writing, the phase θ_i is defined as

$$\theta_i = \mathbf{k}_i \cdot \mathbf{x} - \omega_i t + \delta_i, \quad i = 1, 2. \quad (2.12)$$

The wave number vector points to the propagation direction and horizontal vector \mathbf{x} is defined as,

$$\mathbf{k} = k_x \mathbf{i} + k_y \mathbf{j} = k \cos \beta \mathbf{i} + k \sin \beta \mathbf{j}, \quad (2.13)$$

$$\mathbf{x} = x \mathbf{i} + y \mathbf{j}. \quad (2.14)$$

δ_i and β_i are the initial phase and directional angle for the i th wave component, respectively. The linear dispersion relationship is given by,

$$\omega_i^2 = g k_i \tanh(k_i h), \quad i = 1, 2. \quad (2.15)$$

The corresponding first order surface elevation is

$$\eta^{(1)} = a_1 \cos \theta_1 + a_2 \cos \theta_2. \quad (2.16)$$

Proceeding to the second order approximation, we have to satisfy the following equations

$$\nabla^2 \Phi^{(2)} = 0, \quad (2.17)$$

$$\frac{\partial \Phi^{(2)}}{\partial t} + \frac{1}{2} |\nabla \Phi^{(1)}|^2 + \eta^{(1)} \frac{\partial^2 \Phi^{(1)}}{\partial z t} + g \eta^{(2)} = 0, \quad \text{at } z = 0, \quad (2.18)$$

$$\frac{\partial \eta^{(2)}}{\partial t} + \frac{\partial \Phi^{(1)}}{\partial x} \frac{\partial \eta^{(1)}}{\partial x} + \frac{\partial \Phi^{(1)}}{\partial y} \frac{\partial \eta^{(1)}}{\partial y} - \frac{\partial \Phi^{(2)}}{\partial z} - \eta^{(1)} \frac{\partial^2 \Phi^{(1)}}{\partial z^2} = 0, \quad \text{at } z = 0, \quad (2.19)$$

$$\frac{\partial \Phi^{(2)}}{\partial z} = 0, \quad \text{at } z = -h. \quad (2.20)$$

Eliminating $\eta^{(2)}$ from Equation (2.18) and (2.19), we get

$$\frac{\partial^2 \Phi^{(2)}}{\partial t^2} + g \frac{\partial \Phi^{(2)}}{\partial z} = -\frac{\partial}{\partial t} (|\nabla \Phi^{(1)}|^2) - \eta^{(1)} \frac{\partial}{\partial z} \left(\frac{\partial^2 \Phi^{(1)}}{\partial t^2} + g \frac{\partial \Phi^{(1)}}{\partial z} \right), \quad \text{at } z = 0. \quad (2.21)$$

The second order solution can be satisfied by

$$\begin{aligned} \Phi^{(2)} = & \frac{3 a_1^2 \omega_1 \cosh[2k_1(z+h)]}{8 \sinh^4(k_1 h)} \sin(2\theta_1) + \frac{3 a_2^2 \omega_2 \cosh[2k_2(z+h)]}{8 \sinh^4(k_2 h)} \sin(2\theta_2) \\ & + \frac{a_1 a_2 \omega_2}{2} A_{(-)} \frac{\cosh[|\mathbf{k}_1 - \mathbf{k}_2|(z+h)]}{\cosh(|\mathbf{k}_1 - \mathbf{k}_2|h)} \sin(\theta_1 - \theta_2) \\ & + \frac{a_1 a_2 \omega_2}{2} A_{(+)} \frac{\cosh[|\mathbf{k}_1 + \mathbf{k}_2|(z+h)]}{\cosh(|\mathbf{k}_1 + \mathbf{k}_2|h)} \sin(\theta_1 + \theta_2), \end{aligned} \quad (2.22)$$

where

$$A_{(\mp)} = \mp \frac{k_2 [2\lambda(1 \mp \lambda)(\Gamma \alpha_1 \alpha_2 \pm 1) \mp \lambda^3(\alpha_1^2 - 1) + \alpha_2^2 - 1]}{k_2(1 \mp \lambda)^2 - \alpha_2 |\mathbf{k}_1 \mp \mathbf{k}_2| \tanh(|\mathbf{k}_1 \mp \mathbf{k}_2|h)}, \quad (2.23a)$$

$$\lambda = \frac{\omega_1}{\omega_2}, \quad (2.23b)$$

$$\alpha_i = \coth(k_i h), \quad i = 1, 2, \quad (2.23c)$$

$$\Gamma = \cos(\beta_1 - \beta_2). \quad (2.23d)$$

The solution of $\eta^{(2)}$ can be obtained from Equation (2.18).

$$\begin{aligned}
\eta^{(2)} = & \frac{a_1^2 \omega_1^2}{4g} \left[2 + \frac{3 \cosh(2k_1 h)}{\sinh^4(k_1 h)} - \frac{1}{\sinh^2(k_1 h)} \right] \cos 2\theta_1 \\
& + \frac{a_2^2 \omega_2^2}{4g} \left[2 + \frac{3 \cosh(2k_2 h)}{\sinh^4(k_2 h)} - \frac{1}{\sinh^2(k_2 h)} \right] \cos 2\theta_2 \\
& + \frac{a_1 a_2 k_2}{2\alpha_2} [-(1 - \lambda)A_{(-)} + M_{(-)}] \cos(\theta_1 - \theta_2) \\
& + \frac{a_1 a_2 k_2}{2\alpha_2} [(1 + \lambda)A_{(+)} + M_{(+)}] \cos(\theta_1 + \theta_2), \tag{2.24a}
\end{aligned}$$

where

$$M_{(\mp)} = \lambda^2 + 1 - \lambda(\Gamma\alpha_1\alpha_2 \pm 1). \tag{2.24b}$$

The Bernoulli constant, which is introduced to set the mean water level at $z = 0$, can be shown as

$$C_0 = \sum_{i=1}^2 \frac{a_i^2 k_i}{2} \frac{1}{\sinh 2k_i h}. \tag{2.25}$$

Based on the velocity potential function, we can obtain the hydrodynamic pressure head, velocity and acceleration components up to the second-order. The formulations are given in Appendix A.

In an ocean wave field, there are many free-wave components. The present solutions for hydrodynamic pressure head, velocity and acceleration can be easily extended to multi-component interactions by superposing the interactions among all the wave components.

When two waves are propagating unidirectionally, we have $\beta_1 = 0$ and $\beta_2 = 0$. Thus the multi-directional solutions reduce to unidirectional solutions. It can be showed that the simplified solutions are exactly the same as the unidirectional solutions given by Zhang et al. (1993).

B. Phase Modulation Method

In the case of unidirectional waves, it is found that the truncated solution for the interaction between a short-wave and a long-wave component by the MCM may not converge, if $\varepsilon_1 > \varepsilon_l$ (Zhang et al. 1993). The convergence difficulty of the MCM can be overcome through the use of the PMM (Zhang et al. 1993). The PMM was extended to allow for directional wave interactions in deep water by Hong (1993). Hong's derivation revealed the structure of the solutions for modulated short-wave by a directional long wave. However, his derivation is lengthy, starting in the conformal mapping coordinates and then mapping the solution back to that in Cartesian coordinates. To simplify Hong's derivation, a new modulation perturbation scheme was developed, which directly derives the solution for the modulated directional short-wave component in the Cartesian coordinates (Zhang et al. 1998). The present solution was also extended to allow for intermediate-water depth with respect to the long-wave component. The derivation is described below.

In contrast to the MCM approach, which describes the effects of wave-wave interactions in terms of high order solutions and interprets them as *bound* waves or *forced* waves, the phase modulation approach considers the consequence of wave interactions as the modulation of the short-wave component. Therefore the PMM describes it directly in the solution for the short-wave component. For a directional deep-water short-wave component modulated by an intermediate water-depth long-wave component, we explicitly formulate the modulation in the solutions for the short-wave potential and elevation according to the features discovered by Hong (1993). We then determine the solutions by using the governing equation and boundary conditions.

The total potential and surface elevation can be expressed as a superposition of

the potentials and elevations of a short-wave and a long-wave components,

$$\Phi = \Phi_1 + \Phi_3, \quad (2.26)$$

$$\eta = \eta_1 + \eta_3, \quad (2.27)$$

where the subscripts 1 and 3 stand for the long-wave and short-wave components, respectively.

The governing equation and boundary conditions for Φ are the same as (2.1)–(2.4) except that the bottom boundary condition for the short-wave component is changed to

$$\nabla\Phi_3 \rightarrow 0 \quad \text{as } z \rightarrow -h, \quad (2.28)$$

because the water depth is deep with respect to the short-wave component.

The effect of the interactions on the long-wave component is known to be at most of third-order in wave steepness (Zhang et al. 1993; Hong 1993). Hence, the solution for the long-wave component up to second-order is the same as a single Stokes wave train. By expanding the free surface boundary conditions at the undisturbed long-wave surface and subtracting the undisturbed long-wave surface boundary conditions, we obtain the governing equation and boundary conditions for the short-wave component, correct to the second order in wave steepnesses,

$$\nabla^2\Phi_3 = 0, \quad -h \leq z \leq \eta_1, \quad (2.29)$$

$$\begin{aligned} \frac{\partial\Phi_3}{\partial t} + g\eta_3 + \nabla\Phi_1 \cdot \nabla\Phi_3 + \frac{\partial^2\Phi_1}{\partial t\partial z}\eta_3 \\ + \frac{1}{2}|\nabla\Phi_3|^2 + \frac{\partial^2\Phi_3}{\partial t\partial z}\eta_3 = 0 \quad \text{at } z = \eta_1, \end{aligned} \quad (2.30)$$

$$\begin{aligned} \frac{\partial\eta_3}{\partial t} - \frac{\partial\Phi_3}{\partial z} + \nabla_h\Phi_1 \cdot \nabla_h\eta_3 + \nabla_h\Phi_3 \cdot \nabla_h\eta_1 \\ - \frac{\partial^2\Phi_1}{\partial z^2}\eta_3 + \nabla_h\Phi_3 \cdot \nabla_h\eta_3 - \frac{\partial^2\Phi_3}{\partial z^2}\eta_3 = 0 \quad \text{at } z = \eta_1, \end{aligned} \quad (2.31)$$

$$\nabla\Phi_3 \rightarrow 0 \quad \text{as } z \rightarrow -h, \quad (2.32)$$

where ∇_h is the horizontal gradient operator. The last two terms on the left-hand-sides of (2.30) and (2.31) are of second order and describe the interaction of the short-wave component with itself. Thus, they only contribute to the second harmonic of the short-wave component and consequently can be ignored in the derivation of the modulations of the first harmonic of the short-wave component. The remaining non-linear terms in (2.30) and (2.31) represent the interaction between the long-wave and short-wave components. Because the second harmonic of the short-wave component is of the second-order, the modulational effects on the second harmonic are of the third-order. The solution for the second harmonic of short-wave component up to second order is the same as a single Stokes wave and its derivation is omitted here for brevity.

From Hong's study (1993), we anticipate that the modulated short-wave component potential and elevation can be expressed as,

$$\Phi_3 = A_3 f_A e^{k_3 f_k} \sin \tilde{\theta}_3, \quad (2.33)$$

$$\eta_3 = a_3 (1 + \varepsilon_1 b \cos \theta_1) \cos \tilde{\theta}_3, \quad (2.34)$$

where

$$f_A = 1 + \varepsilon_1 \tau \cos \theta_1, \quad (2.35a)$$

$$f_k = z - a_1 \cos \theta_1 + \varepsilon_1 z \cos \theta_1 \sum_{j=0}^J \gamma_j (k_1 z)^j, \quad (2.35b)$$

$$\tilde{\theta}_3 = k_{3x} x + k_{3y} y - \omega_3 t + \delta_3 + k_3 a_1 \sin \theta_1 \sum_{j=0}^{J+1} \rho_j (k_1 z)^j, \quad (2.35c)$$

$$\tilde{\tilde{\theta}}_3 = k_{3x} x + k_{3y} y - \omega_3 t + \delta_3 + k_3 a_1 \rho_0 \sin \theta_1 + \Delta \varepsilon_1 \sin \theta_1, \quad (2.35d)$$

A_3 is the average potential amplitude of the short-wave component, f_A represents the modulation of the potential amplitude, f_k denotes the effects of the changes of

the short wavenumber and the relative still water level (swl) due to the presence of the long-wave component. $\tilde{\theta}_3$ and $\tilde{\tilde{\theta}}_3$ are the modulated phases for the modulated velocity potential and surface elevation, respectively. They are modeled as the sum of the corresponding linear phase and the modulation by the long-wave component, b stands for the modulation of the elevation amplitude and Δ is the phase shift between the elevation phase and the potential phase at the free surface. The parameters, ρ , γ , τ and b , can be further expanded in terms of the frequency ratio of the long-wave to the short-wave component, λ ,

$$\rho_j = \sum_{n=0}^{2(J+1)-2j} \lambda^n \rho_{jn}, \quad \gamma_j = \sum_{n=0}^{2J-2j} \lambda^n \gamma_{jn}, \quad \tau = \sum_{n=0}^{2J} \lambda^n \tau_n, \quad b = \sum_{n=0}^{2J} \lambda^n b_n, \quad (2.36)$$

where the summation is set to be zero if its upper limit is negative.

Since the phase modulation approach is intended to describe the interactions between short-wave and long-wave components with quite different wavelengths, λ is expected to be relatively small. Generally speaking, it is smaller than 0.5. Theoretically, the summations in (2.35b), (2.35c) and (2.36) can be extended to infinity. But in reality they have to be truncated at a finite order. Equations (2.35b) and (2.35c) involve double summations and the series in both summations converge if $\lambda \ll 1$, because the magnitude of $k_1 z$ also depends on λ . Therefore, to achieve an accuracy at certain order of λ for the solutions of the potential and elevation, the truncations of the summations in (2.35b), (2.35c) and (2.36), have to be made consistently. For example, the truncation of ρ_j in (2.36) depends on the subscripts j and the truncation integer J in the summations of (2.35b) and (2.35c). The reasons are elaborated below.

To ensure the value of the short-wave potential to be nontrivial, the absolute value of its exponential index $k_3 z$ can not be too large. i.e. the index should be of $O(1)$. Because of $k_1/k_3 = \alpha_1 \lambda^2$, we have $|k_1 z| \sim O(\alpha_1 \lambda^2)$. Furthermore, because the

water depth is intermediate with respect to the long-wave component, $\alpha_1 \sim O(1)$. Hence, $|k_1 z| \sim O(\lambda^2)$ and $(k_1 z)^j \sim O(\lambda^{2j})$. If ρ_j is truncated at $2(J+1) - 2j$, then ρ_{j+1} should be truncated at $2(J+1) - 2(j+1)$. As a result, $\rho_j(k_1 z)^j$ and $\rho_{j+1}(k_1 z)^{j+1}$ are accurate up to the same order of λ , i.e. $O(\lambda^{2(J+1)})$. Likewise, the truncation in γ_j should be made accordingly. Since τ and b only involve a single summation, to achieve the same accuracy their summations in (2.36) are truncated at $2J$. As a result, the truncated solutions for the short-wave potential and elevation are accurate up to $O(\varepsilon_1 \lambda^{2J})$.

Substituting (2.33) into the Laplace equation (2.29), we obtain

$$\nabla^2 \Phi_3 = E e^{k_3 f k} \sin \bar{\theta}_3 \cos \theta_1 \varepsilon_1 k_3^2 + F e^{k_3 f k} \cos \bar{\theta}_3 \sin \theta_1 \varepsilon_1 k_3^2 = 0, \quad (2.37)$$

and the coefficients E and F are given by

$$\begin{aligned} E = & -\lambda^4 \alpha_1^2 \tau - 2\Gamma \sum_{j=0}^J \rho_j(k_1 z)^j + \lambda^2 \alpha_1 \left[1 - \sum_{j=0}^J \gamma_j(k_1 z)^{j+1} \right] \\ & + 2 \sum_{j=0}^J (j+1) \gamma_j(k_1 z)^j + \lambda^2 \alpha_1 \sum_{j=0}^{J-1} (j+1)(j+2) \gamma_{j+1}(k_1 z)^j, \end{aligned} \quad (2.38a)$$

$$\begin{aligned} F = & -2\lambda^2 \alpha_1 \Gamma \tau + 2\Gamma \left[1 - \sum_{j=0}^J \gamma_j(k_1 z)^{j+1} \right] - \lambda^2 \alpha_1 \sum_{j=0}^J \rho_j(k_1 z)^j \\ & + 2 \sum_{j=1}^J j \rho_j(k_1 z)^{j-1} + \lambda^2 \alpha_1 \sum_{j=1}^{J-1} j(j+1) \rho_{j+1}(k_1 z)^{j-1}, \end{aligned} \quad (2.38b)$$

where Γ was defined in (2.23d). Splitting (2.37) with respect to $\sin \bar{\theta}_3$ and $\cos \bar{\theta}_3$, we have $E = F = 0$, which can be satisfied by further letting all coefficients of the terms, $(k_1 z)^m$, be zero. For $E = 0$, we get the following equations,

$$O(1) : -2\Gamma \rho_0 - \lambda^4 \alpha_1^2 \tau + \lambda^2 \alpha_1 + 2\gamma_0 + 2\lambda^2 \alpha_1 \gamma_1 = 0, \quad (2.39a)$$

$$\begin{aligned} O(k_1^m z^m) : & -2\Gamma \rho_m - \lambda^2 \alpha_1 \gamma_{m-1} + 2(m+1) \gamma_m \\ & + \lambda^2 \alpha_1 (m+1)(m+2) \gamma_{m+1} = 0, \quad m = 1, 2, \dots \end{aligned} \quad (2.39b)$$

Similarly, for $F = 0$,

$$O(1) : 2\Gamma - 2\lambda^2\alpha_1\tau\Gamma - \lambda^2\alpha_1\rho_0 + 2\rho_1 + 2\lambda^2\alpha_1\rho_2 = 0, \quad (2.40a)$$

$$\begin{aligned} O(k_1^m z^m) : & -2\Gamma\gamma_{m-1} - \lambda^2\alpha_1\rho_m + 2(m+1)\rho_{m+1} \\ & + \lambda^2\alpha_1(m+1)(m+2)\rho_{m+2} = 0, \quad m = 1, 2, \dots \end{aligned} \quad (2.40b)$$

Equations (2.39) and (2.40) can be further expanded in terms of λ . From (2.39a), we obtain the following hierarchy equations

$$O(1) : -2\Gamma\rho_{00} + 2\gamma_{00} = 0, \quad (2.41a)$$

$$O(\lambda) : -2\Gamma\rho_{01} + 2\gamma_{01} = 0, \quad (2.41b)$$

$$O(\lambda^2) : -2\Gamma\rho_{02} + \alpha_1 + 2\gamma_{02} + 2\alpha_1\gamma_{10} = 0, \quad (2.41c)$$

$$O(\lambda^3) : -2\Gamma\rho_{03} + 2\gamma_{03} + 2\alpha_1\gamma_{11} = 0, \quad (2.41d)$$

$$O(\lambda^n) : -2\Gamma\rho_{0,n} + 2\gamma_{0,n} - \alpha_1^2\tau_{n-4} + 2\alpha_1\gamma_{1,n-2} = 0, \quad n \geq 4. \quad (2.41e)$$

Similarly, (2.39b) can be expanded as, for $m = 1, 2, \dots$,

$$O(1) : -2\Gamma\rho_{m,0} + 2(m+1)\gamma_{m,0} = 0, \quad (2.42a)$$

$$O(\lambda) : -2\Gamma\rho_{m,1} + 2(m+1)\gamma_{m,1} = 0, \quad (2.42b)$$

$$\begin{aligned} O(\lambda^n) : & -2\Gamma\rho_{m,n} - \alpha_1\gamma_{m-1,n-2} + 2(m+1)\gamma_{m,n} \\ & + (m+1)(m+2)\alpha_1\gamma_{m+1,n-2} = 0, \quad n \geq 2. \end{aligned} \quad (2.42c)$$

In the same way, (2.40a) is further expanded as

$$O(1) : 2\rho_{10} + 2\Gamma = 0, \quad (2.43a)$$

$$O(\lambda) : 2\rho_{11} = 0, \quad (2.43b)$$

$$O(\lambda^n) : 2\rho_{1n} - 2\alpha_1\tau_{n-2}\Gamma - \alpha_1\rho_{0,n-2} + 2\alpha_1\rho_{2,n-2} = 0, \quad n \geq 2. \quad (2.43c)$$

and so does (2.40b) for $m = 1, 2, \dots$

$$O(1) : -2\Gamma\gamma_{m-1,0} + 2(m+1)\rho_{m+1,0} = 0, \quad (2.44a)$$

$$O(\lambda) : -2\Gamma\gamma_{m-1,1} + 2(m+1)\rho_{m+1,1} = 0, \quad (2.44b)$$

$$O(\lambda^n) : -2\Gamma\gamma_{m-1,n} - \alpha_1\rho_{m,n-2} + 2(m+1)\rho_{m+1,n} \\ + (m+1)(m+2)\alpha_1\rho_{m+2,n-2} = 0, \quad n \geq 2. \quad (2.44c)$$

The simultaneous equations (2.41)–(2.44) can be used to express all coefficients of ρ_j and γ_j in terms of $\rho_0(\rho_{00}, \rho_{01}, \dots, \rho_{0n})$, and $\tau(\tau_0, \tau_1, \tau_2, \dots, \tau_n)$. Later, it will be shown that the coefficients ρ_0 and τ can be determined using the free-surface boundary conditions. Thus, the solution for the potential can be obtained. The procedures of expressing the coefficients of ρ_j and γ_j in terms of ρ_0 and τ are detailed below.

To facilitate the description of the procedures, the coefficients ρ_{ij} and γ_{ij} are described as the elements of the matrices ρ and γ , respectively, as in (2.45), where i and j are the row and column numbers of the element, respectively. The i th row elements in ρ and γ matrices belong to the coefficients ρ_i and γ_i , respectively, as shown in (2.36). The description is divided in two parts,

$$\{\rho\} = \begin{pmatrix} \rho_{00} & \rho_{01} & \rho_{02} & \dots & \rho_{0n} \\ \rho_{10} & \rho_{11} & \rho_{12} & \dots & \rho_{1n} \\ \rho_{20} & \rho_{21} & \rho_{22} & \dots & \rho_{2n} \\ \vdots & \vdots & \vdots & \ddots & \vdots \\ \rho_{n0} & \rho_{n1} & \rho_{n2} & \dots & \rho_{nn} \end{pmatrix}, \quad \{\gamma\} = \begin{pmatrix} \gamma_{00} & \gamma_{01} & \gamma_{02} & \dots & \gamma_{0n} \\ \gamma_{10} & \gamma_{11} & \gamma_{12} & \dots & \gamma_{1n} \\ \gamma_{20} & \gamma_{21} & \gamma_{22} & \dots & \gamma_{2n} \\ \vdots & \vdots & \vdots & \ddots & \vdots \\ \gamma_{n0} & \gamma_{n1} & \gamma_{n2} & \dots & \gamma_{nn} \end{pmatrix}. \quad (2.45)$$

(a) Noticing that the solutions for ρ_{10} and ρ_{11} are explicitly given by (2.43a) and (2.43b), the solutions for all elements in the first two columns ($j = 0$ and 1) of the matrices ρ and γ can be expressed in terms of ρ_{00} or ρ_{01} (which are the elements of

ρ_0) explicitly by solving the simultaneous equations (2.41a), (2.41b), (2.42a), (2.42b), (2.44a) and (2.44b). The results are given below.

$$\rho_{i,j} = \begin{cases} \frac{\rho_{0j}}{i!} \Gamma^i, & i \text{ is even and } i \geq 2, j = 0, 1, \\ -\frac{\Gamma^i}{i!}, & i \text{ is odd and } i \geq 2, j = 0, \\ 0, & i \text{ is odd and } i \geq 2, j = 1. \end{cases} \quad (2.46)$$

$$\gamma_{i,j} = \begin{cases} \frac{\rho_{0j}}{(i+1)!} \Gamma^{i+1}, & i \text{ is even and } 0, i \geq 0, j = 0, 1, \\ -\frac{\Gamma^{i+1}}{(i+1)!}, & i \text{ is odd and } i > 0, j = 0, \\ 0, & i \text{ is odd and } i > 0, j = 1. \end{cases} \quad (2.47)$$

(b) The remaining elements in the matrices ρ and γ are expressed in the recursive relations. There are three rules for obtaining these recursive relations based on the simultaneous equations (2.41c)–(2.41e), (2.42c), (2.43c) and (2.44c). First, an element either ρ_{ij} or γ_{ij} can always be calculated in terms of $\rho_{i'j'}$ and $\gamma_{i'j'}$ if $2i+j > 2i'+j'$. Reminding that the first subscript i implies the corresponding element multiplied by $(k_1 z)^i$ which is of $O(\lambda^{2i})$ and the second subscript j indicates the multiplication of λ^j , the combination of the two subscripts, $2i+j$, indicates the order of λ associated with the corresponding element. Hence, this rule is expected because in a perturbation method the coefficients associated with higher order terms should be solved in terms of coefficients associated with lower order terms. However, there exists a scenario: in each of the above equations there are two elements which belong to the same matrix and whose combinations of the subscripts $(2i+j)$ are the same and the largest. Hence, the second rule for deriving the recursive relations is how to decide which of the two elements is treated as an unknown. When the two elements in an equation has the same greatest combined value of the subscripts, i.e. $2i+j = 2i'+j'$, then the element has a greater second subscript j ($j > j'$) is calculated based on the element of a smaller

second subscript. The reason why the element with a smaller second subscript j' is always known earlier than the one with a greater second subscript j is because the elements in the first two columns of the matrices (ρ and γ) have already been solved as described in part (a). Therefore, for the elements with the same combined value of the two subscripts, the recursive relations for the elements propagates from the left to the right of the matrix. Finally, as shown in (2.42c), two elements $\rho_{m,n}$ and $\gamma_{m,n}$ have exactly the same subscripts and their combination are the greatest. Thus, the third rule for obtaining the recursive relations is that $\gamma_{m,n}$ is calculated based on the results of $\rho_{m,n}$. This is because that the calculation of the corresponding $\rho_{m,n}$ can be made without knowing $\gamma_{m,n}$ in advance as indicated by (2.44c).

According to the above three rules, the order for calculating the elements in the matrices ρ and γ is determined and summarized in (2.48). The number at the location of an element indicates the relative sequence to be calculated in using the recursive relations. For clearness of printing, the corresponding elements are not printed. It should be reminded that the elements in the first row of ρ are treated as known and the elements in the first two columns in both matrices have been given in (2.46) and (2.47).

$$\{\rho\} = \begin{pmatrix} \rho_{00} & \rho_{01} & \rho_{02} & \rho_{03} & \rho_{04} & \rho_{05} & \rho_{06} & \rho_{07} & \rho_{08} & \dots \\ \rho_{10} & \rho_{11} & (1) & (2) & (4) & (6) & (9) & (12) & (16) & \dots \\ \rho_{20} & \rho_{21} & (3) & (5) & (8) & (11) & (15) & \dots & & \\ \rho_{30} & \rho_{31} & (7) & (10) & (14) & \dots & & & & \\ \rho_{40} & \rho_{41} & (13) & (17) & \dots & & & & & \end{pmatrix}, \quad (2.48a)$$

$$\{\gamma\} = \begin{pmatrix} \gamma_{00} & \gamma_{01} & (1) & (2) & (4) & (6) & (9) & (12) & (16) & (20) & \dots \\ \gamma_{10} & \gamma_{11} & (3) & (5) & (8) & (11) & (15) & (19) & \dots & & \\ \gamma_{20} & \gamma_{21} & (7) & (10) & (14) & (18) & \dots & & & & \\ \gamma_{30} & \gamma_{31} & (13) & (17) & \dots & & & & & & \\ \gamma_{40} & \gamma_{41} & (21) & \dots & & & & & & & \end{pmatrix}. \quad (2.48b)$$

Substituting η_3 and Φ_3 into the boundary conditions (2.30) and (2.31) and collecting the terms of the same order in terms of the wave steepness, ε_1 , we obtain the following equations

$$O(1) : A_3\omega_3 = a_3g, \quad (2.49a)$$

$$O(\varepsilon_1) : -A_3\omega_3\tau - A_3k_3k_1^{-1}\omega_1(\rho_0 - \alpha_1\Gamma) + a_3g(b - \alpha_1^{-1}) = 0, \quad (2.49b)$$

$$A_3\omega_1\tau - a_3g\Delta = 0. \quad (2.49c)$$

$$O(1) : a_3\omega_3 = A_3k_3, \quad (2.50a)$$

$$O(\varepsilon_1) : -A_3k_3(\tau + \gamma_0) + a_3(\omega_3b + \omega_1\Delta) + a_3k_3k_1^{-1}\omega_1(\rho_0 - \alpha_1\Gamma) = 0, \quad (2.50b)$$

$$-A_3k_3(\Gamma + \rho_1) + a_3\omega_3\Delta + a_3\omega_1(b - \alpha_1) = 0. \quad (2.50c)$$

where the equations of $O(\varepsilon_1)$ are further split with respect to the factors of $\sin\theta_1$ and $\cos\theta_1$. Equation (2.49a) renders the relationship between the average potential and elevation amplitudes,

$$A_3 = \frac{a_3g}{\omega_3}. \quad (2.51)$$

Combining (2.49a) and (2.50a), the linear dispersion relationship is obtained: $\omega_3^2 = gk_3$. Equation (2.49c) relates the phase shift Δ to τ ,

$$\Delta = \lambda\tau. \quad (2.52)$$

Noticing $\lambda^2 = \alpha_1^{-1}k_1/k_3$, (2.52) and (2.51), equations (2.49b), (2.50b) and (2.50c) can be reduced to,

$$-\tau - \lambda^{-1}\alpha_1^{-1}\rho_0 + \lambda^{-1}\Gamma + b - \alpha_1^{-1} = 0, \quad (2.53a)$$

$$-\tau - \gamma_0 + b + \alpha_1^{-1}\lambda^{-1}\rho_0 + \lambda^2\tau - \lambda^{-1}\Gamma = 0, \quad (2.53b)$$

$$-\Gamma - \rho_1 + \lambda\tau + \lambda b - \lambda\alpha_1 = 0. \quad (2.53c)$$

Although the short-wave potential Φ_3 depends on many parameters (ρ_n and γ_n) which can be determined using the recursive relations in terms of ρ_0 and τ , it is noted that only ρ_0 , ρ_1 and γ_0 appear in the free-surface boundary conditions. Subtracting (2.53a) from (2.53b) and subtracting (2.53c) divided by λ from (2.53b), we eliminate b from the system of equations.

$$-\gamma_0 + \alpha_1^{-1} + 2\alpha_1^{-1}\lambda^{-1}\rho_0 + \lambda^2\tau - 2\lambda^{-1}\Gamma = 0, \quad (2.54a)$$

$$-2\tau - \gamma_0 + \alpha_1^{-1}\lambda^{-1}\rho_0 + \lambda^{-1}\rho_1 + \alpha_1 + \lambda^2\tau = 0. \quad (2.54b)$$

Since γ_0 and ρ_1 can be calculated in terms of ρ_0 and τ using the recursive relations resulting from the Laplace equation as described earlier, there are only two unknowns τ and ρ_0 in (2.54) and hence they can be solved exactly. The procedures are briefly described below.

Equations (2.54a) and (2.54b) can be further perturbed in terms of λ . From (2.54a), we have the following set of equations,

$$O(\lambda^{-1}) : \rho_{00} = \Gamma\alpha_1, \quad (2.55a)$$

$$O(\lambda^0) : \rho_{01} = \frac{1}{2}(\alpha_1\gamma_{00} - 1), \quad (2.55b)$$

$$O(\lambda) : \rho_{02} = \frac{1}{2}\alpha_1\gamma_{01}, \quad (2.55c)$$

$$O(\lambda^n) : \rho_{0n+1} = \frac{\alpha_1}{2}(\gamma_{0n} - \tau_{n-2}), \quad n \geq 2. \quad (2.55d)$$

Similarly, equation (2.54b) can be perturbed into the following set of equations,

$$O(\lambda^{-1}) : \rho_{00} = -\alpha_1 \rho_{10} = \alpha_1 \Gamma, \quad (2.56a)$$

$$O(\lambda^0) : \tau_0 = \frac{1}{2}(\alpha_1^{-1} \rho_{01} + \rho_{11} - \gamma_{00} + \alpha_1), \quad (2.56b)$$

$$O(\lambda) : \tau_1 = \frac{1}{2}(\alpha_1^{-1} \rho_{02} + \rho_{12} - \gamma_{01}), \quad (2.56c)$$

$$O(\lambda^n) : \tau_n = \frac{1}{2}(\alpha_1^{-1} \rho_{0n+1} + \rho_{1n+1} - \gamma_{0n} - \tau_{0n-2}), \quad n \geq 2. \quad (2.56d)$$

Noticing $\gamma_{00} = \Gamma \rho_{00} = \Gamma^2 \alpha_1$ from (2.41a) and (2.56a), ρ_{01} can be calculated from (2.55b). Because ρ_{00} and ρ_{01} are known, the coefficients γ_{ij} ($j = 0, 1$) and ρ_{ij} ($j = 0, 1; i \geq 2$) can be obtained using the recursive relations shown in (2.46) and (2.47). Then ρ_{02} and τ_0 can be calculated as shown in (2.55c) and (2.56b). Based on the recursive relation (2.43c), we obtain

$$\rho_{12} = \alpha_1 \left(\Gamma \tau_0 + \frac{1}{2} \rho_{00} - \rho_{20} \right). \quad (2.57)$$

Then τ_1 can be calculated from (2.56c). The solutions for ρ_{0n+1} and τ_n for $n \geq 2$ can be alternatively obtained from lower to higher n using (2.55d) and (2.56d). In the computation, γ_{0n} and ρ_{1n+1} are computed using the recursive relations described earlier. The solutions for ρ_{ij} ($i \geq 2; j \geq 2$) and γ_{ij} ($j \geq 1$) can also be calculated using the recursive relations. Substituting ρ_{0n} and τ_n ($n = 0, 1, \dots$) into (2.53a), b_n ($n = 0, 1, \dots$) can be calculated.

The final solutions for ρ , γ , τ , and b are presented in Appendix B. The potential and elevation of the modulated first-harmonic short-wave components can be readily obtained from (2.33), (2.34) and (2.35) after ρ , γ , τ , and b have been evaluated. The modulated dynamic pressure head, velocity and acceleration can be derived from the modulated potential and are presented in Appendix C.

C. Hybrid Wave Model

When applying the HWM to an ocean wave field, its spectrum is usually divided into three regions: pre-long, powerful and restriction regions from low to high frequency as sketched in Figure 1. The powerful region involves all free-wave components with relatively significant wave energy and is further divided into four bands, i.e. long-wave band one (L1) and two (L2) and short-wave band 1 (S1) and 2 (S2), starting from low to high in the frequency domain. For most ocean waves, the spectral peak is usually located in the band L1. The amplitudes and especially the wave steepnesses of the free-wave components in the pre-long wave region are very small. Hence, the interaction of a free-wave component in the pre-long wave region with any free-wave components is insignificant and hence neglected. It is also assumed that the wave components in the restriction region are mainly the bound-wave components resulting from the interactions among the free-wave components in the wave bands of L1, L2, S1 and S2. Therefore, the cut-off frequency for the free-wave components is that at the end of S2.

Two free-wave components located in the same frequency band or in neighboring bands are relatively close in the frequency domain and hence the interactions between them are calculated using the conventional. While two free-wave components located in two different bands separated by at least one other band are relatively far apart in the frequency domain and, therefore, are calculated using the PMM. Table I presents the interactions between a wave spectrum with two long wave bands L1,L2 and two short wave bands S1,S2. Details of band division are discussed in Chapter 3.

For simplicity of illustration, we assume that a frequency spectrum for an irregular wave field is divided into three wave bands, say, two long-wave bands (L1 and L2) and one short-wave band (S1), in describing the solution for a wave field

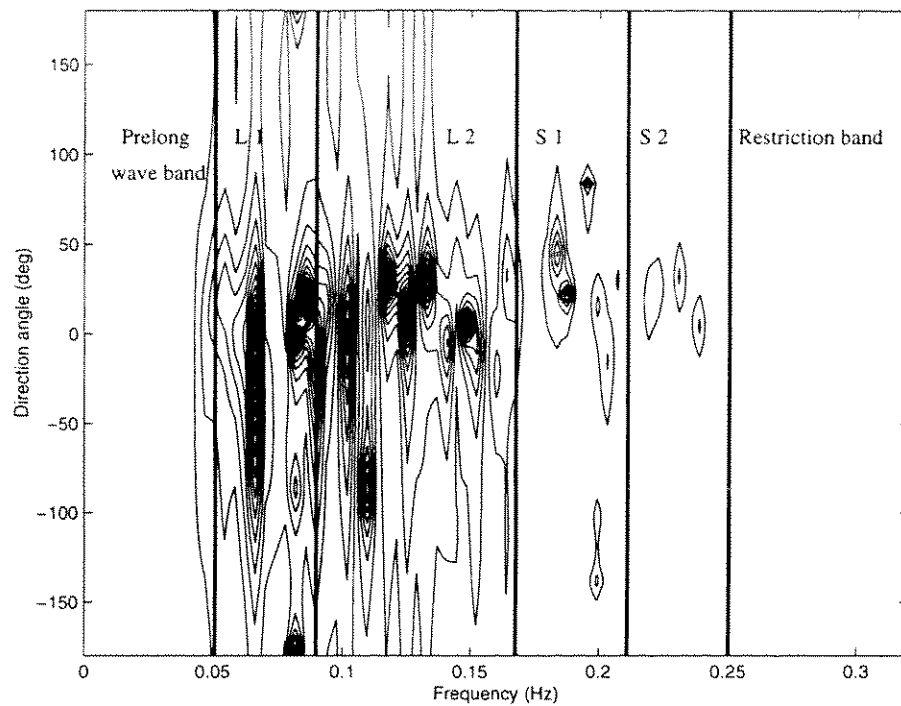


FIGURE 1. Band division of directional hybrid wave model.

Bands	L_1	L_2	S_1	S_2
L_1	M	/	/	/
L_2	M	M	/	/
S_1	P	M	M	/
S_2	P	P	M	M

Table I. Interactions between four wave bands: P: phase modulation method (PMM); M: mode-coupling method (MCM).

of multiple free-wave components. It is straightforward to extend the solution to a wave field consisting of more than three wave bands. Following the earlier discussion, the interactions between the free-wave components in L1 and L2 are calculated using the MCM, likewise, for the interactions between the free-wave components in L2 and S1, respectively, and between the free-wave components in S1. However, the interactions between the two free-wave components located respectively in L1 and S1 are computed using the PMM.

Assuming there are M_1 and M_2 frequency increments in L1 and L2, and N frequency increments in S1, respectively, and there is only one free-wave component at each frequency, the total velocity potential of a directional wave field can be written as

$$\Phi = \Phi_{L1} + \Phi_{L2} + \Phi_{S1L1} + \Phi_{S1L2} + \Phi_{SS}, \quad (2.58)$$

in which Φ_{L1} and Φ_{L2} are the resultant total potentials, including the potentials of all free-wave components in L1 and L2, and the nonlinear interactions between them, Φ_{S1L1} is the potentials of the free-wave components in S1 modulated by those in L1, Φ_{S1L2} is the resultant potential resulting from the nonlinear interactions between L2 and S1, Φ_{SS} is the resultant short-wave potential from interactions between the free-wave components in S1. These potentials can be calculated by:

$$\begin{aligned} \Phi_{L1} + \Phi_{L2} = & \sum_{j=1}^M \left\{ \frac{a_j g \cosh[k_j(z+h)]}{\omega_j \cosh(k_j h)} \sin \theta_j + \frac{3 a_j^2 \omega_j \cosh[2k_j(z+h)]}{8 \sinh^4(k_j h)} \sin(2\theta_j) \right\} \\ & + \sum_{j=2}^M \sum_{i=1}^{j-1} \left\{ \frac{a_i a_j \omega_j}{2} A_{j-i} \frac{\cosh[|\mathbf{k}_j - \mathbf{k}_i|(z+h)]}{\cosh(|\mathbf{k}_j - \mathbf{k}_i|h)} \sin(\theta_j - \theta_i) \right. \\ & \left. + \frac{a_i a_j \omega_j}{2} A_{j+i} \frac{\cosh[|\mathbf{k}_j + \mathbf{k}_i|(z+h)]}{\cosh(|\mathbf{k}_j + \mathbf{k}_i|h)} \sin(\theta_j + \theta_i) \right\}, \quad (2.59) \end{aligned}$$

where $M = M_1 + M_2$, A_{j-i} and A_{j+i} are the same as $A_{(-)}$ and $A_{(+)}$ given in (2.23a)

except that the subscripts 1 and 2 are replaced by i and j , respectively.

$$\Phi_{S1L1} = \sum_{j=M+1}^{M+N} \Phi_j, \quad (2.60)$$

where Φ_j is determined in the same way as Φ_3 in (2.33) except that the modulation factors f_A and f_k , and the modulated phase $\tilde{\theta}_j$ need to be extended to allow for the modulation by multiple long-wave components in L1,

$$f_{Aj} = 1 + \sum_{i=1}^{M_1} \varepsilon_i \tau_{ij} \cos \theta_i, \quad (2.61)$$

$$f_{kj} = z - \sum_{i=1}^{M_1} \left\{ a_i \cos \theta_i + \varepsilon_i z \cos \theta_i \left[\sum_{l=0}^J \gamma_{lij} (k_i z)^l \right] \right\}, \quad (2.62)$$

$$\tilde{\theta}_j = k_{jx}x + k_{jy}y - \omega_j t + \delta_j + \sum_{i=1}^{M_1} \left[k_j a_i \sin \theta_i \sum_{l=0}^J \rho_{lij} (k_l z)^l \right], \quad (2.63)$$

where the subscripts of i and j stand for i th long-wave component and j th short-wave component, respectively.

$$\begin{aligned} \Phi_{S1L2} + \Phi_{SS} = & \sum_{j=M+1}^{M+N} \frac{3 a_j^2 \omega_j \cosh[2k_j(z+h)]}{8 \sinh^4(k_j h)} \sin(2\theta_j) + \left(\sum_{j=M+2}^{M+N} \sum_{i=M+1}^{j-1} + \sum_{j=M_1+1}^M \sum_{i=M+1}^{M+N} \right) \\ & \left\{ \frac{a_i a_j \omega_j}{2} A_{j-i} \frac{\cosh[|\mathbf{k}_j - \mathbf{k}_i|(z+h)]}{\cosh(|\mathbf{k}_j - \mathbf{k}_i|h)} \sin(\theta_j - \theta_i) \right. \\ & \left. + \frac{a_i a_j \omega_j}{2} A_{i+j} \frac{\cosh[|\mathbf{k}_j + \mathbf{k}_i|(z+h)]}{\cosh(|\mathbf{k}_j + \mathbf{k}_i|h)} \sin(\theta_j + \theta_i) \right\}. \end{aligned} \quad (2.64)$$

Similarly, we can express the surface elevation η as

$$\eta = \eta_{L1} + \eta_{L2} + \eta_{S1L1} + \eta_{S1L2} + \eta_{SS}, \quad (2.65)$$

where the right-hand-side terms are corresponding to the potentials with the same subscripts in (2.58).

$$\eta_{L1} + \eta_{L2} = \sum_{j=1}^M a_j \cos \theta_j$$

$$\begin{aligned}
& + \sum_{j=1}^M \frac{a_j^2 \omega_j^2}{4g} \left[2 + \frac{3 \cosh(2k_j h)}{\sinh^4(k_j h)} - \frac{1}{\sinh^2(k_j h)} \right] \cos 2\theta_j \\
& + \sum_{j=2}^M \sum_{i=1}^{j-1} \left\{ \frac{a_i a_j k_j}{2\alpha_j} [-(1-\lambda)A_{j-i} + M_{j-i}] \cos(\theta_j - \theta_i) \right. \\
& \quad \left. \frac{a_i a_j k_j}{2\alpha_j} [(1+\lambda)A_{i+j} + M_{i+j}] \cos(\theta_i + \theta_j) \right\}. \tag{2.66}
\end{aligned}$$

$$\eta_{S1L1} = \sum_{j=M+1}^{M+N} a_j \left(1 + \sum_{i=1}^{M_1} \varepsilon_i b_{ji} \cos \theta_i \right) \cos \tilde{\theta}_j, \tag{2.67}$$

where b_{ji} is the value b for j th short-wave component modulated by i th long-wave component and

$$\tilde{\theta}_j = k_{jx}x + k_{jy}y - \omega_j t + \delta_j + \sum_{i=1}^M k_j a_i \rho_{0ij} \sin \theta_i + \sum_{i=1}^M \varepsilon_i \Delta_{ij} \sin \theta_i, \tag{2.68}$$

in which ρ_{0ji} and Δ_{ij} are the coefficients ρ_0 and Δ of j th short-wave component modulated by i th long-wave component, respectively.

$$\begin{aligned}
\eta_{S1L2} + \eta_{SS} = & \sum_{j=1}^N \frac{a_j^2 k_j}{2} \cos 2\theta_j + \left(\sum_{j=M+2}^{M+N} \sum_{i=M+1}^{j-1} + \sum_{j=M_1+1}^M \sum_{i=M+1}^{M+N} \right) \\
& \times \left\{ \frac{a_i a_j k_j}{2\alpha_j} [-(1-\lambda)A_{j-i} + M_{j-i}] \cos(\theta_j - \theta_i) \right. \\
& \left. + \frac{a_i a_j k_j}{2\alpha_j} [(1+\lambda)A_{i+j} + M_{i+j}] \cos(\theta_i + \theta_j) \right\}. \tag{2.69}
\end{aligned}$$

The HWM solutions for pressure, velocity and acceleration can be readily derived from the velocity potential, and are presented in the Appendix C.

CHAPTER III

PREDICTION OF WAVE KINEMATICS

Existing capabilities of predicting kinematics under regular wave conditions have been found to be within the accuracy ($\sim 5\%$) of inherent errors in the laboratory measurements (Dean 1990). But, wave kinematics under irregular ocean waves is not just a simple superposition of wave kinematics of each regular wave component. Linear superposition may be quite wrong if applied to predict wave kinematics above the still water level (swl) because the contribution of short-wave components is exaggerated due to the exponential factor of e^{kz} .

Many stretching and extrapolation methods of computing the irregular wave kinematics have been proposed. However they are based on empirical modifications of linear wave theory and usually lack sound theoretical grounds. Laboratory and field data have shown that these methods may either underestimate or overestimate wave kinematics above the swl (Donelan et al. 1992). Moreover, these modification methods are still controversial among hydrodynamicists (Sobey 1990).

The nonlinear solution of the MCM considers the wave-wave interactions as *bound* waves which are introduced to correct the leading-order solutions. However, the truncated solution may not be convergent if $\varepsilon_1 > \varepsilon_l$ (Zhang et al. 1993). For instance, considering wave kinematics above the swl, the second-order solution can be greater than the already exaggerated leading-order short wave kinematics. The truncated MCM solution may thus be divergent and may not correctly predict the irregular wave kinematics, specially wave kinematics above the swl.

The PMM is an alternative to the MCM. In the case of a long- and short-wave component interaction, it directly considers the modulation of a short-wave component by long-wave components in its leading-order solution. In other words, the

second-order interaction between a short-wave and long-wave component is included in the solution for the modulated short-wave component. The short wave is assumed to ride on the surface of the long-wave component, the leading-order of the short wave kinematics considers the vertical distance with respect to the long-wave surface due to the presence of the long wave component. Figures 2 demonstrates the resultant horizontal velocity of a short wave and a long wave. The PMM considers the vertical distance of the short-wave component with respect to the long-wave surface while leading-order MCM considers with respect to the swl. We observe that the leading-order MCM over predicts the kinematics of the short-wave component at the long-wave peak and underestimates at the long-wave trough.

Hu et al.(1995) used the second-order MCM to compute the wave kinematics under unidirectional irregular waves. It was found that the predicted wave kinematics above the swl by the MCM was very sensitive to the cutoff frequency. The inclusion of high frequency wave components by choosing a higher cutoff frequency, greatly changed the wave kinematics in the vicinity of the swl. They then concluded that the large change was caused by the inclusion of additional high frequency short-wave components. The large change of kinematics of a wave field should result from the inclusion of additional large wave energy. It is not likely that the inclusion of trivial energy wave components causes a big change of wave kinematics. Hence, their conclusion explanation was incorrect. The contradiction between the inclusion of additional trivial energy and large change in wave kinematics is mainly due to the divergence of the MCM solution.

In this chapter, we will theoretically and numerically show the divergence of the MCM solution under the condition of $\varepsilon_1 > \varepsilon_l$. Predictions of wave kinematics by the MCM and PMM are compared. The sensitivity of wave kinematics prediction by the MCM solution with respect to the cutoff frequency is also discussed. Prediction of

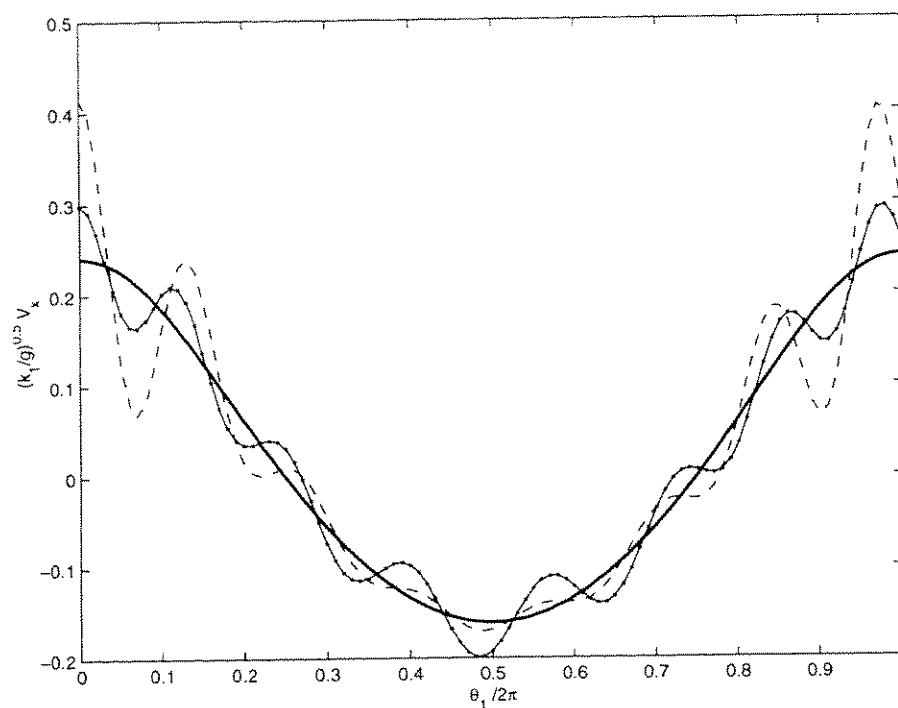


FIGURE 2. Resultant horizontal velocity in x -direction of a long wave and a short wave obtained by the PMM (—•—), (---) is the leading order solution of short wave velocity by the MCM, long wave velocity is (—) for reference, the velocity is nondimensionalized by $(k_1/g)^{0.5}$.

unidirectional irregular wave kinematics by the directional HWM is compared with that by the unidirectional HWM that has been verified with laboratory measurements.

A. Two Wave Components Interaction

When $\varepsilon_1 \ll \varepsilon_l < 0.5$, the PMM is identical to the MCM up to third order in wave steepness. On the other hand, when ε_1 approaches ε_l , the MCM converges slowly and eventually diverges when $\varepsilon_1 > \varepsilon_l$. (Zhang et al. 1993; Chen & Zhang 1997)

Two free-wave components are considered with the long-wave component at the frequency of 0.1328 Hz and a short-wave component at 0.2148 Hz. The water depth is 145.0 m, which is of intermediate-depth water condition to the long wave and deep-water condition to the short wave. The wave length ratio of the short to long wave ε_l is 0.3822. Steepness of the long-wave component is 0.10. The short-wave component has an amplitude of 0.5382 m and its steepness is 0.10 also. The direction angel is 0 degree for the long wave component and 30 degree for the short one.

Both the MCM and PMM are used to predict the surface elevation at horizontal position (-11.6 m,0.0 m). Velocity and acceleration components are also predicted at the same location but 3.0 m below the swl. Figure 3 shows virtually identical time series of surface elevation, horizontal velocity component in x -direction and vertical acceleration component predicted by of these two approaches.

However, when ε_1 approximates ε_l , that is, the long-wave component is steep and the short-wave component is much shorter than the long-wave component in wavelength, the MCM solution may diverge while the PMM remains convergent. The non-convergence of the MCM solution can be theoretically demonstrated as following. For simplicity, the wave directionality is excluded and water depth is set to be deep for both long and short-wave components as these two factors are not crucial to the

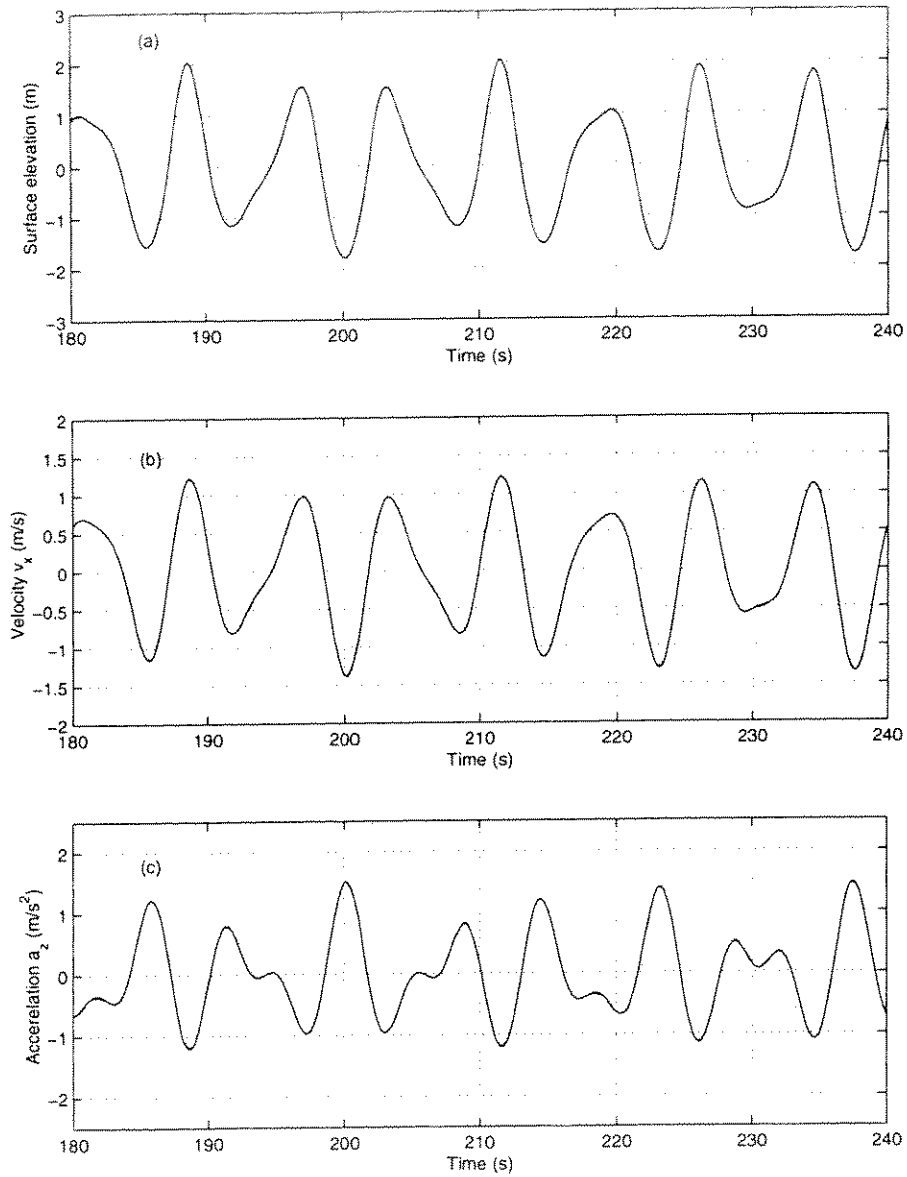


FIGURE 3. Comparison between the MCM (—) and the PMM (---) for a dual free-wave spectrum with $\varepsilon_1 = 0.10$, $\varepsilon_l = 0.3822$: (a) surface elevation; (b) horizontal velocity in x direction; (c) vertical acceleration.

divergence of MCM solution.

The nonlinear potential functions by the MCM solution is simplified from the directional intermediate-depth solution by setting the directional angles of zero and $\alpha_i = 1, (i=1,2)$,

$$\Phi = \sum_{i=1}^2 \frac{a_i g}{\omega_i} e^{k_i z} \sin \theta_i - a_1 a_2 \omega_2 e^{(k_2 - k_1)z} \sin(\theta_2 - \theta_1), \quad (3.1)$$

where subscript 1, 2 stand for long- and short-wave component respectively. Leading-order velocities are the spatial derivatives of the leading-order potential. For instance, the horizontal velocity is

$$u^{(1)} = a_1 \omega_1 e^{k_1 z} \sin \theta_1 + a_2 \omega_2 e^{k_2 z} \sin \theta_2. \quad (3.2)$$

When the short-wave component becomes relatively short and the long-wave component is relatively steep, the leading-order velocity of the short wave component under the long-wave peak is obviously over estimated because of the factor of $e^{k_2 z} (z \sim \eta_1)$.

The second-order velocities are the derivative of the second-order potential. We still use the horizontal velocity as an example,

$$u^{(2)} = -a_1 a_2 \omega_2 (k_2 - k_1) e^{(k_1 - k_2)z} \cos(\theta_2 - \theta_1). \quad (3.3)$$

Noticing that $\frac{k_1}{k_2} = \varepsilon_l$, we rewrite the second-order horizontal velocity as

$$u^{(2)} = \varepsilon_1 a_2 \omega_2 (1 - \varepsilon_l^{-1}) e^{k_2 z} e^{-k_1 z} \cos(\theta_2 - \theta_1). \quad (3.4)$$

We consider the kinematics near long-wave crest, i.e. $z \sim a_1$ or $k_1 z \sim \varepsilon_1$. The amplitude of above second-order velocity can be approximated by

$$|u^{(2)}| = a_2 \omega_2 e^{k_2 z} \left(-\varepsilon_1 \varepsilon_l^{-1} + \varepsilon_1 \right) \left[1 - \varepsilon_1 + \frac{1}{2} \varepsilon_1^2 + O(\varepsilon_1^3) \right], \quad (3.5)$$

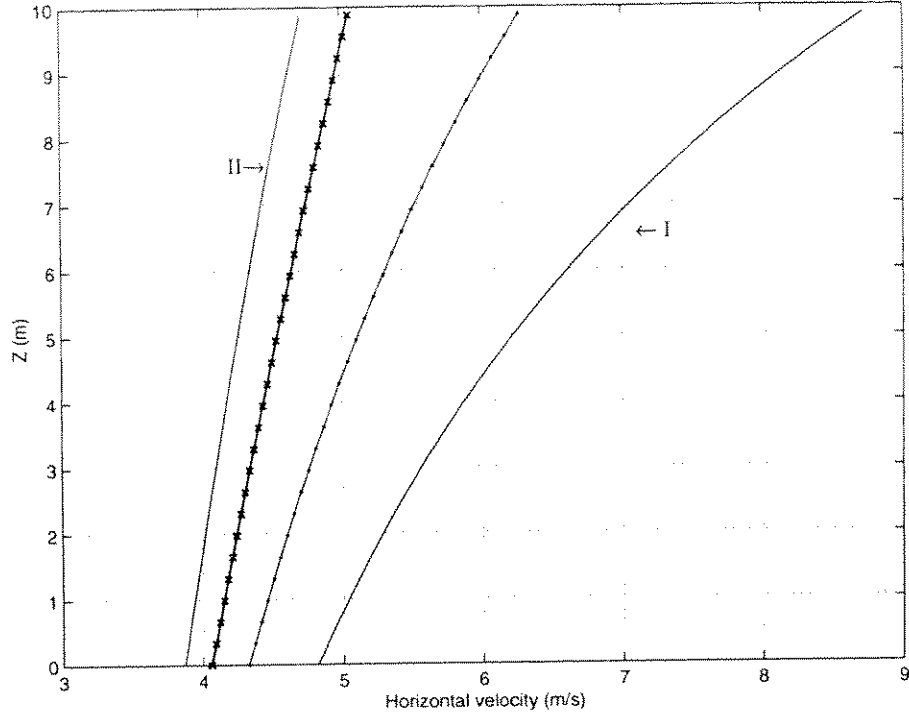


FIGURE 4. Comparison between MCM (---) and PMM (—●—) for a dual free-wave spectrum with $\varepsilon_1 = 0.20$, $\varepsilon_l = 0.139$, x -direction horizontal velocity profiles of the long and short waves up to the leading order (I —) and the second order (II —), and the long-wave velocity only (— x —).

where $e^{k_1 z}$ is approximated by its truncated Taylor expansion. The dominant terms of Equation (3.5) are $(-\varepsilon_1 \varepsilon_l^{-1} + \varepsilon_1) a_2 \omega_2 e^{k_2 z}$. Under the condition of $\varepsilon_1 > \varepsilon_l$, $-\varepsilon_1 \varepsilon_l^{-1} a_2 \omega_2 e^{k_2 z}$ is bigger than the leading-order term $a_2 \omega_2 e^{k_2 z}$ which is over estimated. The second term $\varepsilon_1 a_2 \omega_2 e^{k_2 z}$ is much smaller than the leading-order term because of the factor of ε_1 . Then the correction of second order under this condition is greater than the exaggerated leading-order solution, which indicates that the MCM solution becomes divergent.

To numerically demonstrate this point, a set of steep dual free-wave components are studied with the long-wave component at the frequency of 0.07422 Hz and a

short-wave component at 0.1992 Hz. The water depth remains 145.0 m. The short to long wave length ratio ε_l is 0.1390 and steepness of the long-wave component is 0.20. The direction angle is 15 degree for the long wave and - 15 degree for the short wave. Figure 4 shows the x -direction velocity under the resultant wave crest where the short- and long-wave crests coincide. The resultant horizontal velocity of the long wave and the leading-order short wave predicted by the MCM solution is much greater than the horizontal velocity induced by the long wave only. Although the contribution from the leading-order short wave is exaggerated because of the factor $e^{k_2 z}$ ($z \sim \eta_1$), the increase in the resultant horizontal velocity is consistent with our intuition because under the resultant crest both wave components are in the same phase. However, when the resultant horizontal velocity is computed up to second order, i.e. including the contribution from the bound-wave components, the resultant horizontal velocity is found to be smaller than the horizontal velocity induced by the long wave only. This indicates the overall contribution to the resultant horizontal velocity from the short-wave component is out of phase with respect to the elevation of the short-wave component. This contradicts to both our intuition and experimental observations. In contrast, the solution of the PMM up to second order gives physically reasonable description for the short-wave velocity. Figure 5 shows the horizontal velocity of same two wave components except that the short-wave component is now 180 degree out of phase of the long wave, i.e. the elevation of the short wave is in its trough phase when that of the long wave reaches its peak phase. Hence the horizontal velocity of short-wave component should be opposite to the long wave resultant velocity. The results of the MCM shows, however, the short-wave velocity is in the same direction as the long-wave component. It implies the short wave has an positive horizontal velocity at its trough. This is again against the intuition and experimental observations. Nevertheless, the PMM shows the short wave contributes an out of phase velocity,

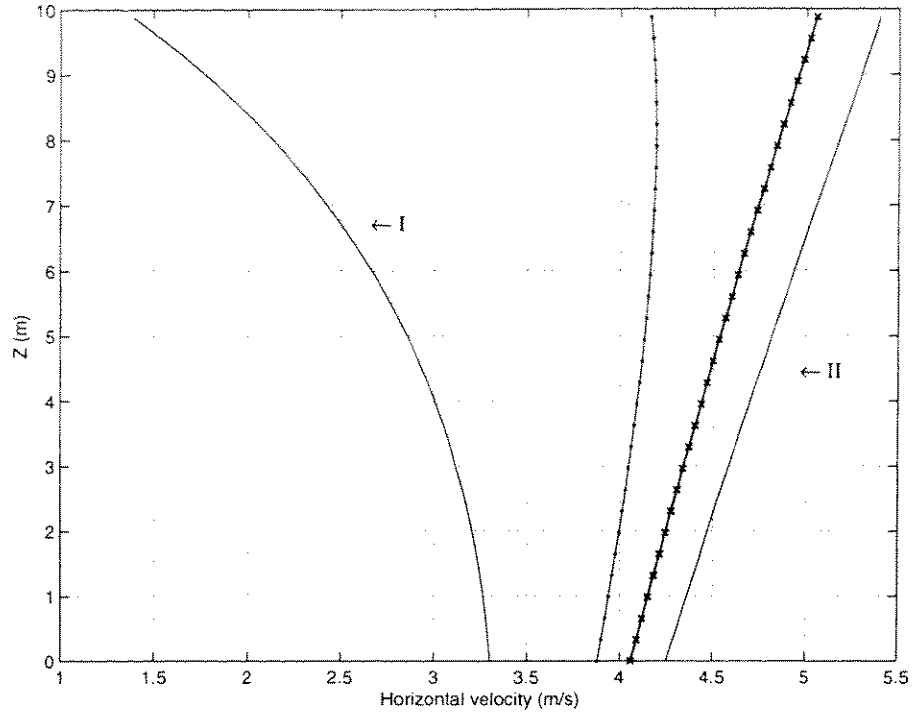


FIGURE 5. Same as Figure 4 except the short wave is 180 degree out of phase of the long-wave component.

which agrees with our intuition and observations.

The above numerical examples show that when $\varepsilon_1 > \varepsilon_l$ the prediction of wave kinematics by the MCM is divergent. The predictions become more divergent when $\varepsilon_1 \gg \varepsilon_l$ as the second-order bound-wave contribution is much bigger than the leading-order solution. For instance, assume a long wave of steepness of $\varepsilon_1 = 0.10$, a short wave component whose frequency is 9 times of that of the long wave. The wave length ratio is $1/81$ if we assume both the wave components are of deep-water condition. Then the dominant second-order solution of short-wave component is about 8 times bigger than the already exaggerated leading-order solution. In summary, the MCM is only valid for narrow-banded spectral interactions. For broad-banded wave spectra, it is necessary to use the PMM to compute the wave-wave interactions of relatively

far-apart wave components .

B. Wave Spectrum Prediction

Analytical wave spectra are usually formulated based on measured ocean wave data. For instance, Pierson-Moskowitz spectrum (Pierson & Moskowitz 1964) is one of the best known wave spectra. Huang (1990), Tayfun (1990) and Zhang et al. (1996) argued that an analytical wave spectrum is actually a resultant spectrum, which is composed of leading-order and higher-order wave-wave interactions. If the nonlinearity is considered only up to second order in wave steepness, the spectrum can be decomposed as

$$S_{\eta} = S_{\eta_1} + S_{\eta_2}, \quad (3.6)$$

where S_{η_1} and S_{η_2} correspond to first- and second-order surface elevation respectively. To compute the second order wave-wave interactions, S_{η_1} should be used instead of S_{η} . Chakrabarti (1987) and Huang (1990) gave a general form of a first-order spectrum also known as *truncated Gamma spectrum*,

$$S_{\eta_1}(f) = \frac{B}{f^p} \exp\left(-\frac{C}{f^q}\right) \quad (\omega \leq \omega_c), \quad (3.7)$$

where B, C, p and q , are four independent parameters of the spectrum. ω_c is the cutoff frequency. Tayfun (1990) studied the relationship between S_{η} and S_{η_1} using second-order MCM wave theory. He argued that for an observed spectrum, such as P-M type spectrum that attenuates as f^{-5} with frequency, the first-order spectrum, $S_{\eta_1}(f)$ can be characterized by spectra that attenuate as f^{-9} with frequency if the second-order contribution is excluded.

Figure 6 shows two truncated Gamma spectra of $p = 9$ and $p = 5$ respectively.

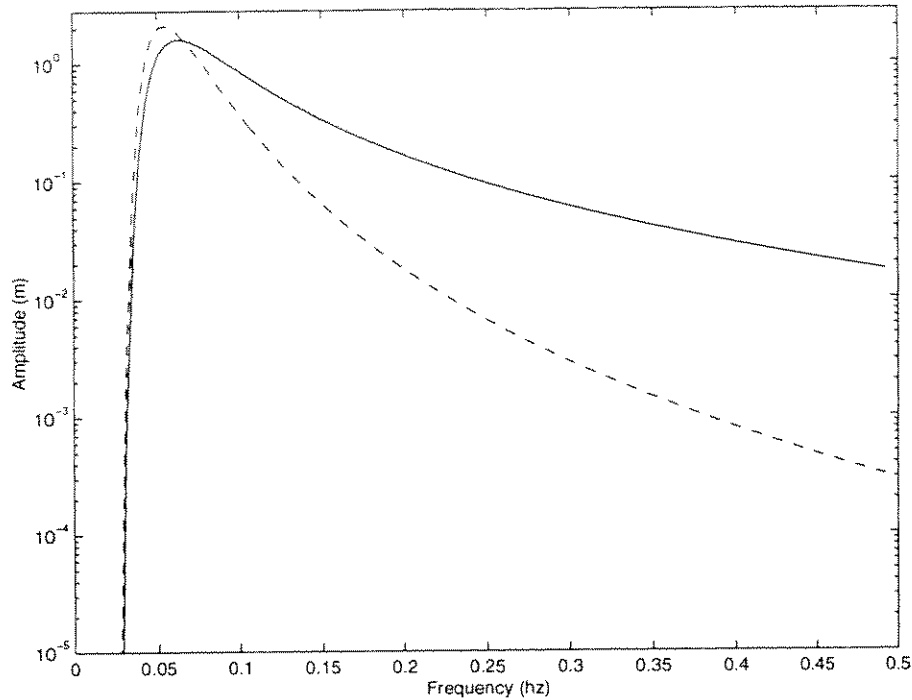


FIGURE 6. Truncated Gamma spectra, (—) : $p=5$, (- - -): $p=9$, nominal steepness $s=0.06$.

Both of the spectra has a nominal steepness of 0.06 defined as

$$s = \frac{\sigma_{\eta_1} \omega_p^2}{g}, \quad (3.8)$$

where $\sigma_{\eta_1}^2$ is the variance of the power spectrum, which is equal to the area under the $S_{\eta_1}(f)$ curve. ω_p is the peak frequency. The amplitude of high frequency wave components in a spectrum of $p = 9$ decay faster than those of a spectrum of $p = 5$. The spectral bandwidth parameter ϵ of the Gamma spectrum of $p = 5$ is 0.444 and 0.2286 of the Gamma spectrum of $p = 9$. ϵ is defined as

$$\epsilon = \sqrt{\frac{m_0 m_2}{m_1^2} - 1}, \quad (3.9)$$

where, m_i is the i th moment of a wave spectrum.

To apply the HWM to compute the wave kinematics of a wave spectrum, it is necessary to divide the wave spectrum into several bands as sketched in Chapter 2. There are two criteria for the band division (Zhang et al. 1996). First, the width of each band should be narrow so that the application of the MCM to the interactions of wave components within the same band is valid. The band width is limited to a maximum equivalent wave steepness, ε_e , which is defined as

$$\varepsilon_e = k_{N_h} \sum_{j=N_l}^J \alpha_j a_j \sin \theta_j, \quad (3.10)$$

where N_l, N_h are the subscripts of the first and last components in the wave band and J is determined from $2k_J \simeq k_{N_h}$. The criteria is that the maximum equivalent wave steepness is much smaller than one

$$\text{Max}(\varepsilon_e) \ll 1. \quad (3.11)$$

The second criterion is that wave components in short wave bands should be of deep water condition. This is due to the assumption of the PMM that the water is considered as deep-water condition with respect to the short-wave components.

In the present study, the long wave bands start where the wave amplitude reaches a certain percentage of the peak wave amplitude, say 5% of the peak amplitude. As the amplitudes of wave components in the pre-long wave band are comparatively small, their interactions with other components in the spectrum are neglected. In other words, only the leading-order contributions of the pre-long band are considered. The first short-wave band starts where the wave component becomes deep wave with respect to the water depth. Then the long wave bands are determined. The last short band ends at the cutoff frequency. If the cutoff frequency is relatively higher, it is necessary to divide the short wave bands into more than two bands. Figure 7 shows a wide spectrum with two long wave bands and four short wave bands.

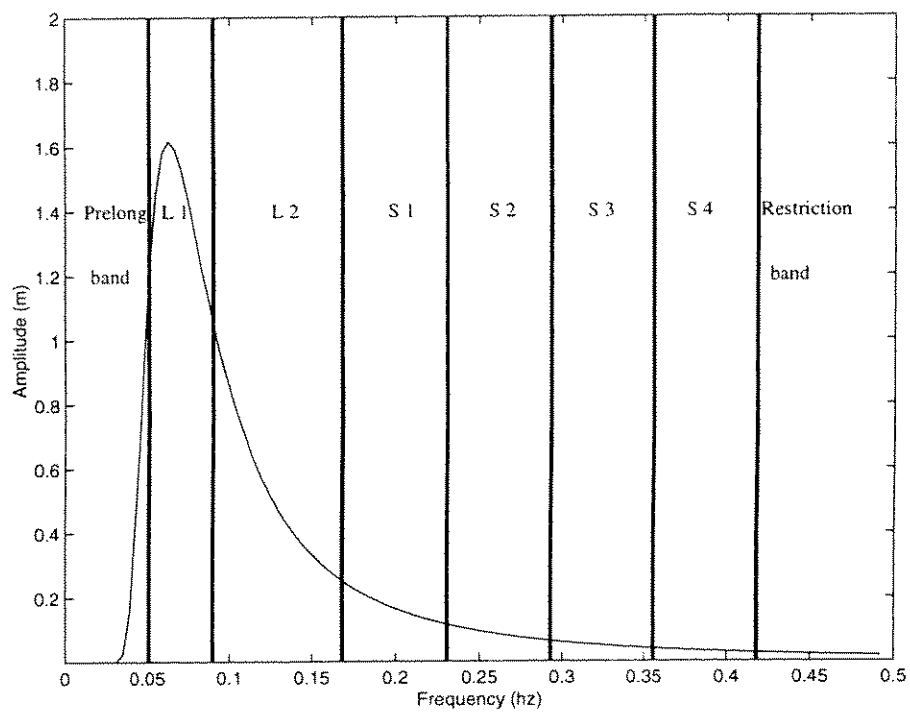


FIGURE 7. Band division of a wide wave spectrum.

Cutoff Frequency	$5\omega_p$	$6\omega_p$	$7\omega_p$	$8\omega_p$	$9\omega_p$
$m_0(m^2)$	11.3760	11.3760	11.3760	11.3760	11.3760

Table II. Zeroth moments of a Gamma spectrum with $5\omega_p$ - $9\omega_p$ cutoff frequency, nominal steepness $s=0.055$.

Hu et al. (1995) used the MCM to study nonlinear wave kinematics of irregular waves of broad and steep spectra. They found that significant change of wave kinematics by the inclusion of high frequency wave components though the included high frequency wave components were of insignificant amplitudes. They concluded that the large change was caused by the leading-order contribution of high frequency wave components. Based on the analysis of two wave components interaction, it is concluded that application of the MCM to predict the wave kinematics of wave components that have quite different wavelengths is invalid. Therefore it is invalid to apply the MCM to predict wave kinematics of broad and steep spectra when the truncated MCM solutions become divergent.

Figure 8 shows predicted horizontal velocity profile under a steep wave crest using the MCM. The spectrum is a Gamma type spectrum of $p = 9$ and nominal steepness 0.055. A range of cutoff frequencies from $5\omega_p$ to $9\omega_p$ are compared, where ω_p is the peak frequency. The profiles predicted by the MCM show oscillating characteristics with respect to the cutoff frequency. The prediction at $9\omega_p$ obviously is divergent.

As we have discussed, the MCM becomes divergent for two wave components if $\varepsilon_1 > \varepsilon_l$. When applying the MCM to a wave spectrum of relatively strong nonlinearity, the second-order interaction by the MCM between long- and short-wave components that have a small wavelength ratio ε_l , may be divergent. Hence the prediction of wave kinematics by the MCM becomes divergent.

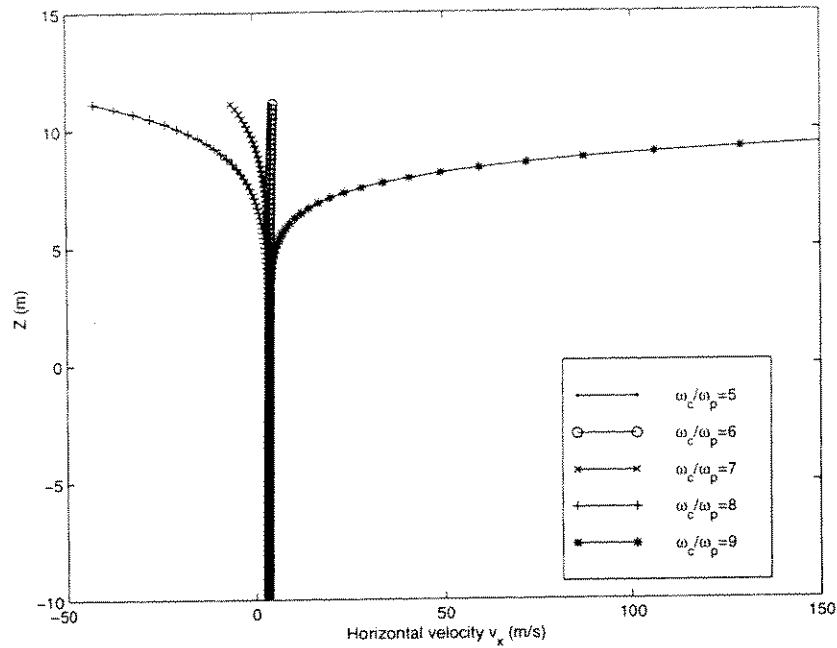


FIGURE 8. Horizontal velocity profile against cutoff frequency by the MCM, nominal steepness $s=0.055$.

From the point of nonlinear wave theory, we have showed earlier the reason of divergence of the MCM under $\varepsilon_1 > \varepsilon_l$ for two wave component interaction. Now we use the principle of energy to show briefly the inconsistency of the predictions by the MCM. Considering a surface elevation time series at a field point, the local potential energy is proportional to the instantaneous surface elevation amplitude in the aspect of linear wave theory. Because the local kinetic energy is proportional to the potential energy, then the change of local kinetic energy should correspond to the instantaneous surface elevation. In other words, it is unlikely that an insignificant change of local surface elevation causes a significant change of local kinetic energy. Now we use a Gamma spectrum of $p = 9$ as an example to show this point. The spectrum has a spectral steepness of 0.055. Table II displays the zeroth moment of

Cutoff Frequency	$5\omega_p$	$6\omega_p$	$7\omega_p$	$8\omega_p$	$9\omega_p$
$\eta(\text{m})$	11.11	11.11	11.12	11.12	11.12

Table III. Surface elevation at $t=54.5$ s of a Gamma spectrum with $5\omega_p$ - $9\omega_p$ cutoff frequency, nominal steepness $s=0.055$.

the Gamma spectrum for different cutoff frequencies. Zeroth moment is obtained by

$$m_0 = \int_0^{\infty} S_{\eta}(f) df. \quad (3.12)$$

It is observed that the wave components of frequency higher than $5\omega_p$ have so small amplitudes that their contribution to m_0 is negligible. Table III displays the instantaneous surface elevation at $t = 54.5$ seconds versus different cutoff frequencies. The change of surface elevation caused by the inclusion of high frequency wave component ($\geq 5\omega_p$) is within 1 cm, which is negligible to the eleven meter total elevation. Therefore the inclusion of the high frequency wave components is unlikely to change the local potential energy notably. The significant change of the local kinetic energy by the inclusion of high frequency wave component is not physically realistic. The divergence of prediction is caused by the improper modeling of MCM for wave components of $\varepsilon_1 > \varepsilon_l$.

Figure 9 depicts the horizontal velocity profile predicted by the PMM. The wave spectrum is the same as that of Figure 8. Because the amplitudes of wave components beyond $5\omega_p$ are very small, the inclusion of higher frequency components has negligible influence on the resultant wave kinematics except for some small changes of velocity at the wave peak.

Therefore, the confusion of Hu et al. (1995) results from the divergence of the MCM solution itself. The divergence of wave kinematics consequently led to divergent

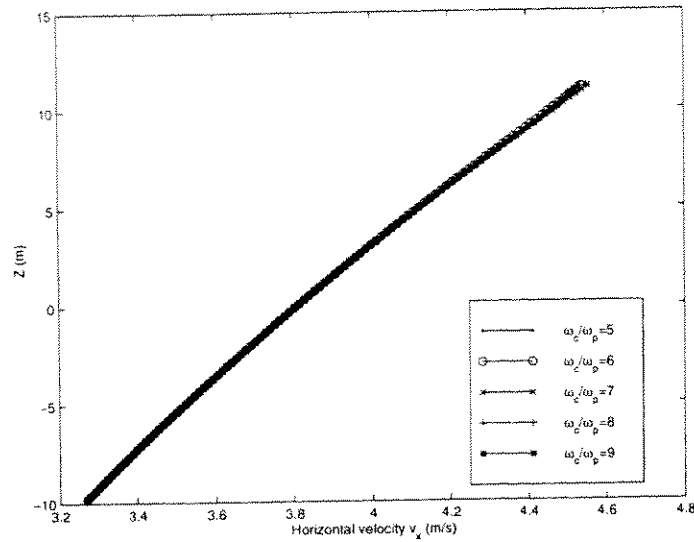


FIGURE 9. Horizontal velocity profile against cutoff frequency by the PMM, same spectrum as Figure 8.

wave forces on the structure in their study. We will discuss this in Chapter 4.

From above analysis, we may conclude that if only a wave spectrum is narrow banded that meets the criteria of the band division in Equation (3.11) can the MCM solution be applied. However, practically speaking, the wave spectra are usually non-narrow spectra, it is necessary to apply the HWM to predict the wave kinematics.

C. Comparison between UHWM and DHWM

Zhang et al. (1996) applied the unidirectional HWM (UHWM) to predict irregular wave kinematics. Excellent agreements have been found between the wave model and laboratory data. Comparison between the predictions of the DHWM and UHWM has shown excellent consistency (Zhang et al. 1998). The free-wave components of the wave trains, shown in Figure 10 are obtained by the decomposition of the surface elevation measurement by a wave gauge located at $x = 0$. Figure 11 demonstrates the time series of horizontal velocity by UHWM and DHWM for a unidirectional wave

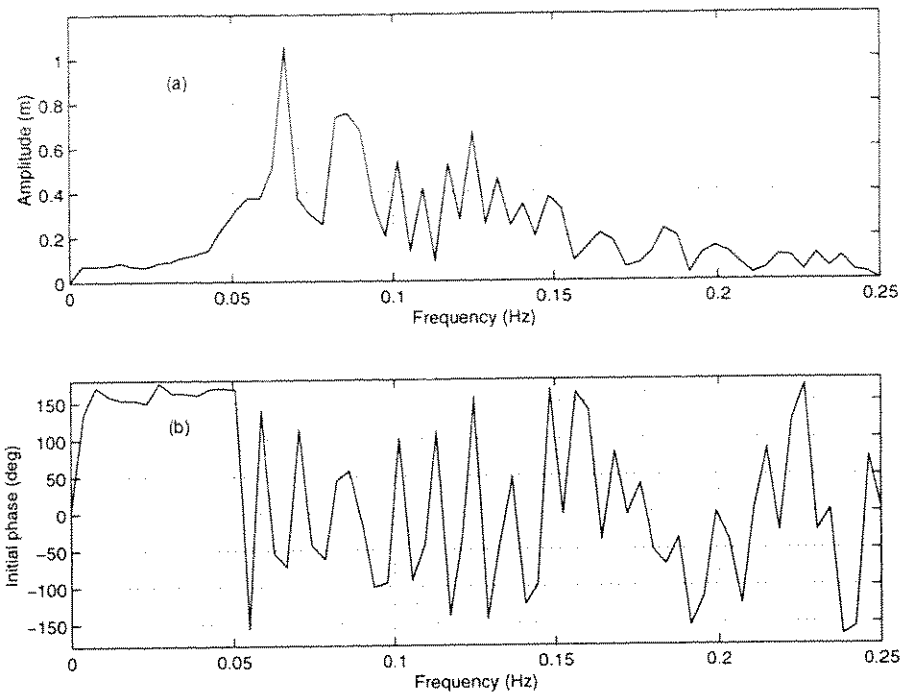


FIGURE 10. Free-wave components consisting of an unidirectional irregular wave trains: (a) amplitudes, (b) initial phases.

field. One finds out excellent agreement between these two models. As in the near future, direct verification between directional wave measurements and the model will be conducted with the advanced directional LDV facility.

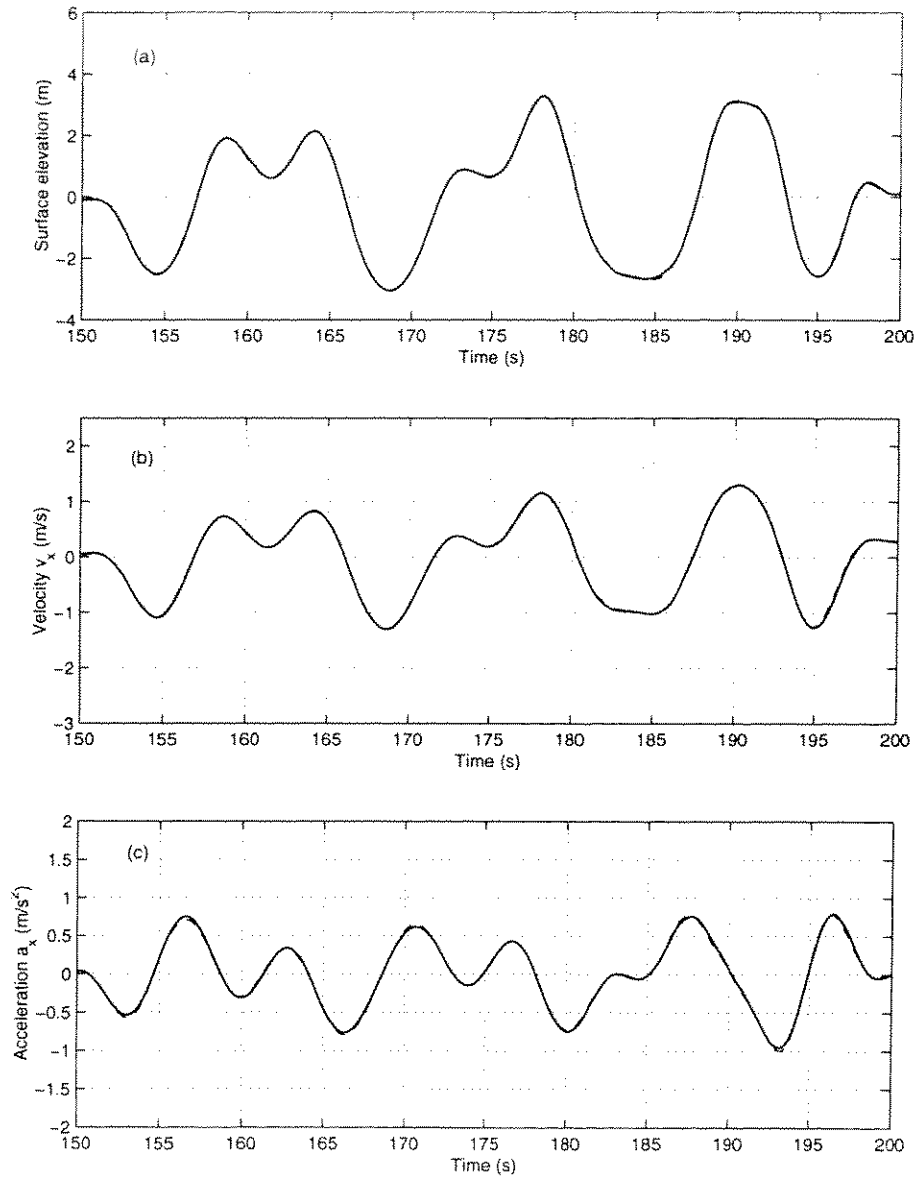


FIGURE 11. Time series of (a) surface elevation (b) horizontal velocity (c) horizontal velocity at location of (10.00,-8.25)m downstream, by DHWM (—) and UHWM (- - -).

CHAPTER IV

WAVE FORCES ON A SLENDER BODY STRUCTURE

An accurate and efficient prediction of wave forces acting on offshore structures is very important in designing offshore structures. For slender body offshore structures, the Morison equation is usually applied to compute the wave forces, which models the wave forces on a structure segment as directly related to the wave kinematics. Therefore, the accuracy of the prediction of wave forces depends on the accuracy of prediction of wave kinematics.

High order *Stokes* wave theory has been applied in the design approach of regular waves. Satisfactory matches have been found between the *Stokes* theory and experimental results (Dean 1990). For the design of structure under irregular waves, linear wave theory may not predict the wave kinematics accurately specially in the surface vicinity and hence may not provide good estimate of wave forces on structures. Many modified methods, such as Wheeler stretching, Linear Extrapolation, etc., have been proposed to tune the wave kinematics near the surface region, where significant discrepancy has been found between the prediction by linear wave theory and field and experiment data. These modifications usually lack sound theoretical grounds and laboratory and field data have shown that these methods may either underestimate or overestimate wave kinematics above the swl (Donelan et al. 1992). The predictive potential and comparative performance of these methods need more detailed evaluation (Sobey 1990).

The MCM is an improvement to the stretching methods. However it was limited to narrow-band wave interactions. As shown in Chapter 3, the MCM is divergent for bichromatic waves if $\varepsilon_1 > \varepsilon_l$. Hu et al.(1995) applied the second-order MCM to study the surface fluctuation and wave nonlinearity effects on slender body structures.

They found quite dramatic change of wave forces on the structure due to the inclusion of high frequency wave components. They concluded that the change was mainly caused by the leading-order contribution from the included short-wave components. As we have shown in Chapter 3, the wave kinematics predicted by the MCM may be divergent and thus the predicted wave forces may be divergent.

Besides the wave model for computing wave kinematics in using the Morison equation, other nonlinear wave effects on computing the wave forces are also important. Linear approach usually integrates the unit wave forces to the swl. Provided that the wave kinematics above swl can be accurately predicted, the wave forces should be integrated up to the instantaneous surface. The consideration of instantaneous surface is commonly referred to as the wave intermittency or surface fluctuation.

In this chapter, we apply the HWM to study the wave intermittency and non-linearity effects on a single degree of freedom (SDOF) slender body structure. Then we will discuss the invalid use of the MCM to predict the wave forces in steep and non-narrow spectra cases by Hu et al. (1995). Comparison between the API (1993) recommended method and HWM is also carried out in the later part of this Chapter. Based on the HWM simulations, important conclusions of the nonlinear effects on the wave forces are given. A desirable cutoff frequency is also proposed based on the HWM.

A. The Morison Equation

The computation of wave force on a structure from the particle motion of the surrounding water by the Morison equation, is based on the assumption that the flow motion is unaffected by the presence of the structure. It has been discovered that the Morison equation is valid for $D/L_c < 0.2$, where D and L_c are the charac-

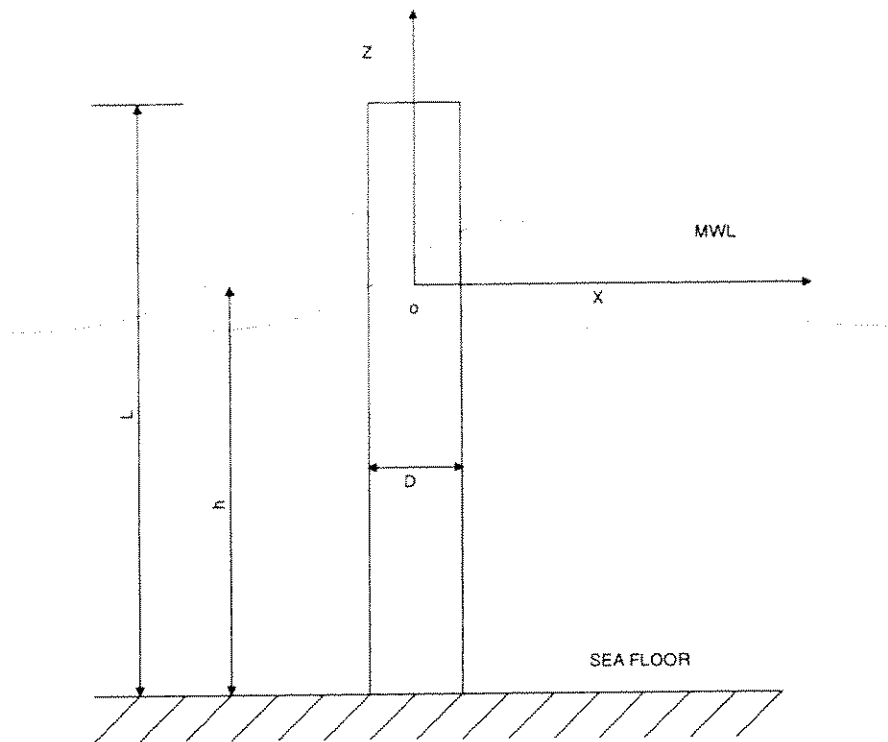


FIGURE 12. Definition sketch of a fix-bottom structure.

teristic dimensions of the structure and wave length respectively. In this study, we consider a simple cylinder structure model and keep the diameter of the structure much smaller than the characteristic wave length at the peak frequency of the wave spectrum. Figure 12 shows the definition of a cylinder structure. L is the total length of structure. h is the water depth, which is assumed to be of intermediate-depth water condition with respect to the peak wave component. The x -positive direction is the wave propagation direction and z -direction points upwards.

The general form of wave forces on a structure segment given by the Morison equation is expressed as

$$\mathbf{f} = \frac{1}{2} C_D \rho D |\mathbf{U} - \mathbf{U}_b| (\mathbf{U} - \mathbf{U}_b) ds + C_M \rho A (\dot{\mathbf{U}} - \dot{\mathbf{U}}_b) ds, \quad (4.1)$$

where, C_D is known as the drag coefficient, C_M inertia coefficient and ρ the density

of water. \mathbf{U} and \mathbf{U}_b are water particle velocity and body motion velocity, $\dot{\mathbf{U}}$ and $\dot{\mathbf{U}}_b$ acceleration vectors of water particle and body motion respectively. A is the cross section area and D the diameter of the section. For a cylindrical structure, D is the diameter for the structure and $A = \frac{\pi D^2}{4}$.

Total wave forces are obtained by a vertical integral of the segmental wave forces. One major purpose of this research is to investigate the nonlinear effects of both free surface fluctuation and the wave nonlinearity on the wave forces using the HWM. To achieve this objective, we compute the wave forces on the structure using:

- (1) liner wave theory, computing the wave forces up to the swl, hereafter subscripted with l ;
- (2) HWM, computing the wave forces up to the swl, hereafter subscripted with nl ;
- (3) HWM, computing the wave forces up to the instantaneous surface, hereafter subscripted with n .

Equation (4.2) shows the forces computed by linear wave theory and Equation (4.3), (4.4) for hybrid wave theory without and with consideration of surface intermittency, respectively.

$$F_l^i = \int_{-h}^0 C_M \rho A (\dot{\mathbf{U}}_l - \dot{\mathbf{U}}_b) dz, \quad (4.2a)$$

$$F_l^d = \int_{-h}^0 \frac{1}{2} C_D \rho D |\mathbf{U}_l - \mathbf{U}_b| (\mathbf{U}_l - \mathbf{U}_b) dz, \quad (4.2b)$$

$$F_{nl}^i = \int_{-h}^0 C_M \rho A (\dot{\mathbf{U}}_n - \dot{\mathbf{U}}_b) dz, \quad (4.3a)$$

$$F_{nl}^d = \int_{-h}^0 \frac{1}{2} C_D \rho D |\mathbf{U}_n - \mathbf{U}_b| (\mathbf{U}_n - \mathbf{U}_b) dz, \quad (4.3b)$$

$$F_n^i = \int_{-h}^{\eta} C_M \rho A (\dot{\mathbf{U}}_n - \dot{\mathbf{U}}_b) dz, \quad (4.4a)$$

$$F_n^d = \int_{-h}^{\eta} \frac{1}{2} C_D \rho D |\mathbf{U}_n - \mathbf{U}_b| (\mathbf{U}_n - \mathbf{U}_b) dz. \quad (4.4b)$$

s	0.01	0.02	0.03	0.04	0.05	0.06
$H_s(m)$	2.548	5.096	7.643	10.191	12.738	15.287

Table IV. Significant wave height against nominal spectral steepness s .

U_1, \dot{U}_1 are the water particle velocity computed by linear wave theory and U_n, \dot{U}_n by the HWM, respectively.

API (1993) recommends Wheeler stretching approach to compute the wave forces on slender body structures. In this study, wave forces using the stretching method are computed up to the instantaneous surface. The predictions of wave forces between linear stretching method and the HWM are compared later in this chapter.

B. Numerical Simulations

To study the nonlinear wave effects, a range of spectra of different nominal steepness are used. The nominal steepness of a spectrum is defined in Equation (3.8). The spectral steepness s ranges 0.01 to 0.06, representing weakly to relatively strong nonlinear waves. The spectrum of steepness 0.06 has a significant wave height equivalent to 100 year Gulf of Mexico Storm (API 1993). Table IV shows the significant wave height versus spectral steepness for the Gamma spectra with the peak period of 16 seconds. The initial phases of the free-wave spectrum are randomly generated. Because the spectrum is unidirectional, the directional angles of all the free-wave components are set to zero.

The wave forces on a SDOF cylinder structure are computed using the aforementioned three different approaches. Simulation is carried out in the time domain with 0.25 second interval and 4096 total time steps. Total wave forces are integrated using a Gauss Quadrature method. Standard deviations of wave forces are denoted as σ^i

and σ^d for inertia, drag wave forces respectively, with subscripts l, nl and n standing for the three different approaches.

C. Effects of Surface Intermittency and Wave Nonlinearity

The ratios of wave force standard deviations between different approaches are computed to investigate the effects of surface fluctuation and wave nonlinearity. They are defined by

$$\mu_1 = \frac{\sigma_l}{\sigma_{nl}}, \mu_2 = \frac{\sigma_{nl}}{\sigma_n}, \mu_3 = \frac{\sigma_l}{\sigma_n}. \quad (4.5)$$

μ_1 is the ratio of wave force standard deviations by linear approach to the HWM of excluding the surface fluctuation. It is introduced to study the effects of wave nonlinearity on the wave forces, more specifically the nonlinear effects without considering the surface fluctuation. μ_2 is introduced to study the effects of surface fluctuation, considering the wave nonlinearity. μ_3 shows the overall effects of both surface intermittency and wave nonlinearity on the wave forces.

Figure 13 plots the simulation results μ_1^d, μ_1^i versus spectral steepness s . From the plot, one finds out that the difference between linear and the HWM without consideration of surface fluctuation is not significant. This is expected because the nonlinear wave interactions are not significant below the swl.

Figure 14 plots the simulation results μ_2^d and μ_2^i versus spectral steepness s . One finds out the surface fluctuation effect is important when the nonlinearity of wave-wave interaction is considered. The surface intermittency effect increases with the spectral steepness. Even if the nonlinear wave-wave interaction is considered, the neglecting of surface intermittency may lead to underestimate of wave forces for this type of structures.

From Figure 14, we also observe that the drag forces are more sensitive to the

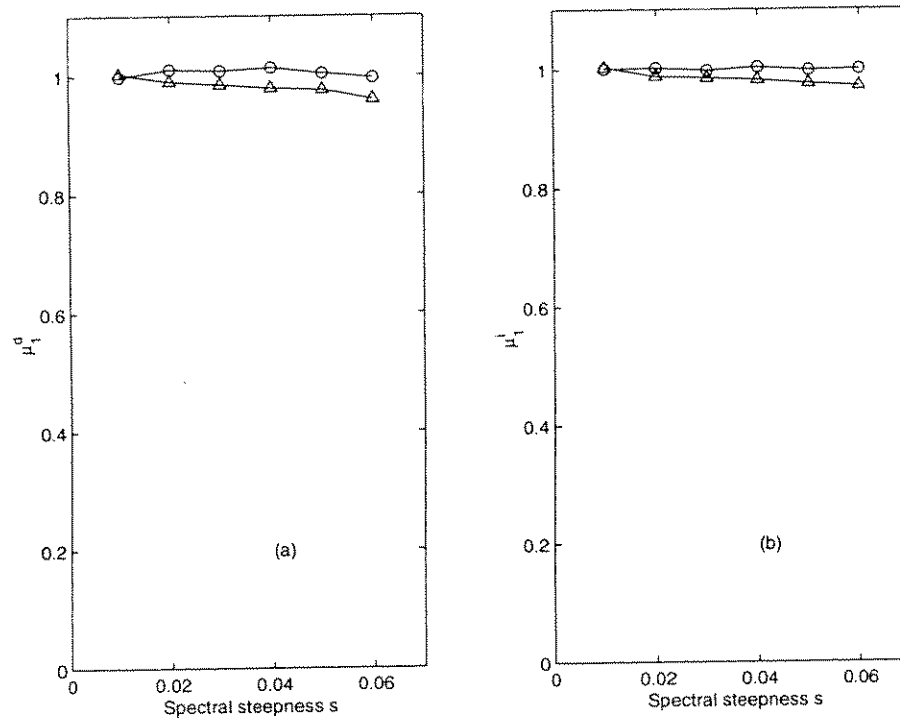


FIGURE 13. μ_1 versus s , (a) drag force (b) inertia force; ($-o-$): Gamma spectrum with $p=9$; ($-\Delta-$): Gamma Spectrum with $p=5$, $\omega_c = 5\omega_p$.

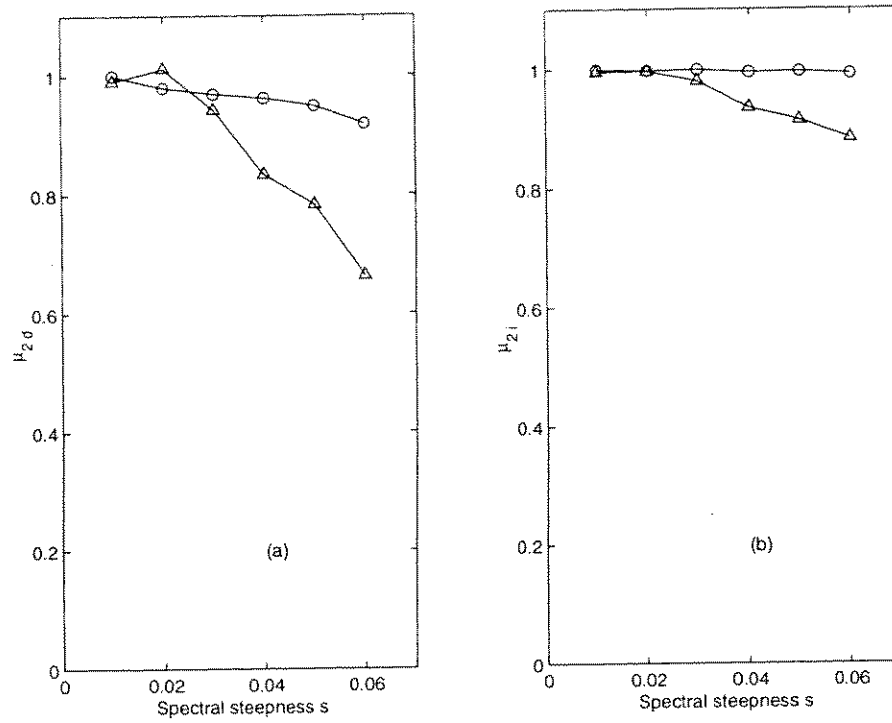


FIGURE 14. μ_2 versus s , (a) drag force (b) inertia force; ($-\circ-$): Gamma spectrum with $p=9$; ($-\triangle-$): Gamma Spectrum with $p=5$, $\omega_c = 5\omega_p$.

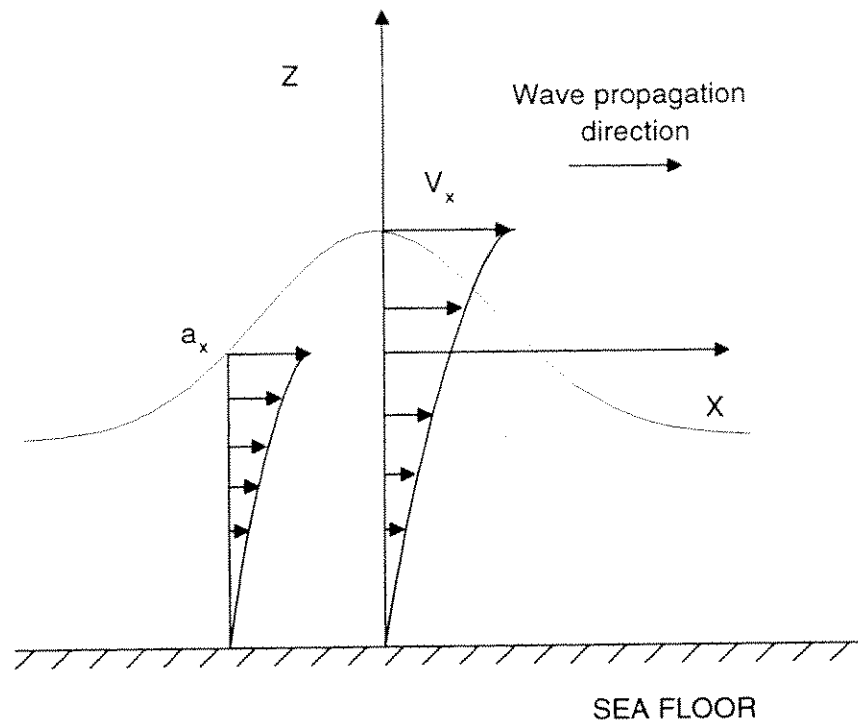


FIGURE 15. Water particle velocity and acceleration in a periodic wave

increase of the spectral steepness than the inertia forces. This can be briefly explained as following. As shown by the Morison equation, the magnitude of the drag force f^d is proportional to the horizontal velocity square. The horizontal velocity is in phase with the surface elevation for a periodic wave. Under the wave peaks the horizontal velocity increases exponentially with the vertical coordinate z , as shown in Figure 15. Because the fluctuation of the surface elevation increases with the spectral steepness or significant wave height, the horizontal velocity therefore increases correspondingly. On the other hand, the horizontal acceleration is 90 degree out of phase with the surface elevation. The maximum acceleration occurs at the swl as shown in Figure 15. The surface fluctuation effects thus are relatively smaller on the acceleration related inertia force.

From Figure 14 we may also observe for different wave spectra the effects of

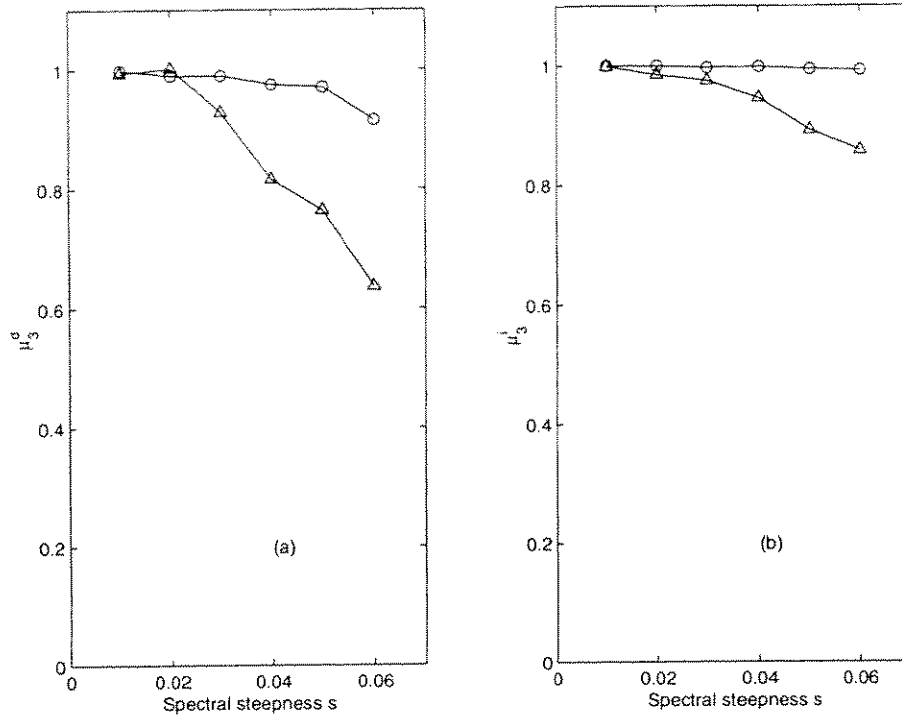


FIGURE 16. μ_3 versus s , (a) drag force (b) inertia force; ($-o-$): Gamma spectrum with $p=9$; ($-\Delta-$): Gamma Spectrum with $p=5$, $\omega_c = 5\omega_p$.

surface fluctuation on wave forces may be different. The gamma spectrum of $p = 5$ represents a relatively broad spectrum, i.e. the powerful band is relatively broad, its nonlinear interactions are stronger compared to the $p = 9$ spectrum.

Figure 16 shows the effects of both wave nonlinearity and surface fluctuation on drag and inertia forces respectively. The surface intermittency and wave nonlinearity effects are important for relatively strong nonlinear waves. The prediction by linear wave theory of drag force is 37% smaller than that by the HWM, for a $p = 5$ Gamma spectrum of nominal steepness 0.06. Also one may observe the overall effects depend on the characteristic of the wave spectrum. For $p = 5$ spectrum, the effects are more significant because of the stronger nonlinear interactions.

From the above simulations, we conclude that the consideration of both wave

nonlinearity and surface fluctuation is necessary in computing the wave forces of this type of structure under relatively strong nonlinear waves. Neglecting of either factor consequently leads to incorrect estimation of wave forces. Linear approach and nonlinear wave approach excluding surface fluctuation effect may considerably underestimate the wave forces on the structure.

However, fixed bottom structure is used in this study to compute the wave forces. For floating type of the structure, like semisubmersible structures, TLP platforms, the diffraction effects may become important (Sarpkaya 1981). More investigations of these effects are needed before we extend this conclusion to other types of offshore structures though we believe that the effects of surface intermittency and wave nonlinearity are still important.

It is also important to point out the effects of surface intermittency and wave nonlinearity depend on the spectrum characteristics. Generally speaking, for a spectrum with relatively broad powerful band, or in other words, a spectrum has a slower decaying factor of frequency, the effects of surface fluctuation and wave nonlinearity are stronger because of the stronger wave-wave interactions between the significant wave components. In the above plots, we have observed the surface fluctuation and wave nonlinearity have more influence on Gamma spectrum of $p = 5$ than that of $p = 9$.

D. Cutoff Frequency

In the computation of spectral wave forces on offshore structures, a cutoff frequency of the wave spectrum needs to be determined. Many computations have shown sensitivity of their computations to the cutoff frequency. Hu et al. (1995) used the MCM to compute wave forces of a SDOF structure using the Morison equa-

tion. Their computation showed tremendously different predictions of wave forces for cutoff frequency $5\omega_p$ and $10\omega_p$ of a same input wave spectrum. They found that the difference was due to the inclusion of short wave components. They concluded that the leading-order wave kinematics of short-wave components was formulated by e^{kz} and the short-wave components dominated the total wave forces when the waves become steeper. nevertheless, their conclusions were incorrect. Firstly, the short-wave components in the tail region of the spectrum have insignificant amplitudes, their contribution to the wave potential energy is small. The inclusion of them is unlikely to cause big change of wave fields. Secondly, wave forces on the structure, is on the other hand, a scale of the energy of the wave field. Greater wave forces on a same structure correspond to stronger wave conditions. The wave forces can not be changed greatly by including the wave components with small energy components, whose contribution to the total potential energy is insignificantly. As we have shown in Chapter 3, the problem was caused by the divergence of the MCM in predicting the wave kinematics.

Now we use both the MCM and HWM to compute the wave forces including the surface intermittency effect. As the MCM approach may predict vertical kinematics profiles that have sudden changes above the swl, we apply a higher order Gauss Quadrature method than the HWM.

We define the ratio of wave force standard deviations of cutoff frequency at $5\omega_p$ to $9\omega_p$ for a same input spectrum, as μ_c ,

$$\mu_c = \frac{\sigma_{n(5\omega_p)}}{\sigma_{n(9\omega_p)}}. \quad (4.6)$$

Figure 17 shows μ_c versus spectral steepness s by the HWM and MCM respectively for a Gamma spectrum of $p = 9$. From the plot, the HWM shows the prediction of wave forces does not depend on the cutoff frequency. The difference of the wave

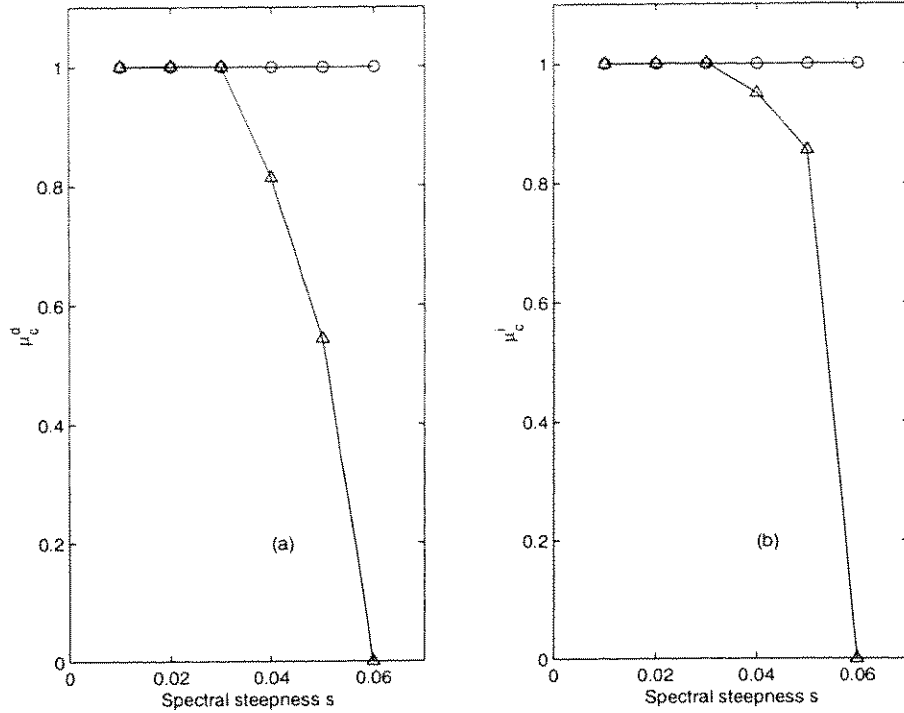


FIGURE 17. μ_c versus s , (a) drag force (b) inertia force; ($-o-$): HWM; ($-\Delta-$): MCM.

forces predicted by the HWM, which is caused by the including of high frequency wave components is negligible. However, the MCM presents sensitive characteristics to the cutoff frequency. For relatively steep wave cases, say $s = 0.06$, the inclusion of short wave components by changing the cutoff frequency from $5\omega_p$ to $9\omega_p$ increases the wave loads by more than a hundred times.

We are not surprised at the predicted results by the MCM. In Chapter 3, we have shown some examples of wave kinematics by the MCM that are very sensitive to the cut off frequency. The sensitivity of the MCM to the cutoff frequency in predicting the wave kinematics and forces is caused by improper modeling of wave-wave interactions of relatively broad and steep wave spectra. But the HWM uses the PMM to model the short- and long- wave interaction and provide consistent predictions.

Based on the above discussions, we may conclude that it is invalid to compute

wave forces based on the wave kinematics predicted by the MCM, of a wave spectrum that is relatively broad and steep. The MCM may render divergent results of wave forces on the structure under strong nonlinear waves. At the meantime, the sensitivity of the MCM to the cutoff frequency in predicting the wave forces is on the other hand an indicator of its incorrect modeling of wave kinematics under broad and steep spectral waves. Intuitive observations also tell us that the inclusion of small amplitudes wave components should not greatly change the wave forces on the structure.

Hu et al. (1995) argued that the determination of cutoff frequency was not clear. Based on the fact that the nonlinear HWM predicts consistent wave forces on the structure with respect to different cut off frequencies, we may propose a desirable cutoff frequency of 3 – 5 times of the peak frequency, for the design practice in offshore engineering field. The determination of the cutoff frequency depends on the characteristic of the design spectrum. If a spectrum has a relatively broad powerful band, the cutoff frequency is proposed to close the upper limit of 5 times of the peak frequency. But for a relatively narrow band spectrum, a cutoff frequency close to 3 times of the peak frequency is adequate. Moreover, the high frequency resultant wave components are contributed mostly from the interactions of waves within the powerful frequency bands. Zhang et al. (1996) argued that after certain frequency, the nonlinear interaction from long wave bands dominates the resultant spectrum in the high frequency region. Hence the inclusion of nonlinear interaction of the long-wave bands may be more important than the inclusion of the free-wave components in the relatively high frequency region. Meanwhile, we remark that it is necessary to include third- and higher-order nonlinearity in the computation for a broad-banded spectrum that is relatively steep as the third- and higher-order interactions from free-wave components near the spectral peak become relatively important. The third- and

higher-order nonlinearity is not considered in this research.

E. Wheeler Stretching Approach

Another widely used approach to compute the wave forces is the stretching method, or called Wheeler stretching method (API 1993). Wave kinematics above the swl is computed using a modified vertical coordinate, which is linearly mapped from the original position by

$$z' = \frac{d(z - \eta)}{d + \eta}, \quad (4.7)$$

where z' is the modified coordinate and z is the original one.

Wave forces are computed using

$$F_w^i = \int_{-h}^{\eta} C_M \rho A (\dot{\mathbf{U}}_w - \dot{\mathbf{U}}_b) dz, \quad (4.8)$$

$$F_w^d = \int_{-h}^{\eta} \frac{1}{2} C_D \rho D |\mathbf{U}_w - \mathbf{U}_b| (\mathbf{U}_w - \mathbf{U}_b) dz. \quad (4.9)$$

where $\dot{\mathbf{U}}_w$ and \mathbf{U}_w are the acceleration and velocity vectors computed by the Wheeler stretching method.

In this study, we also use this method to compute the wave forces and compare them to the results predicted by the HWM. Similarly, we use the time domain simulation and compare the standard deviations of these two methods. The ratio between these two methods is denoted as μ_w ,

$$\mu_w = \frac{\sigma_w}{\sigma_n}. \quad (4.10)$$

Figure 18 plots μ_w versus spectral steepness s . For relatively steep waves, Wheeler stretching tends to underestimate wave loads. For two different Gamma spectra, Wheeler stretching method tends to more underestimate the waves forces of $p = 5$ spectrum than those of the $p = 9$ spectrum. This is because the nonlinear

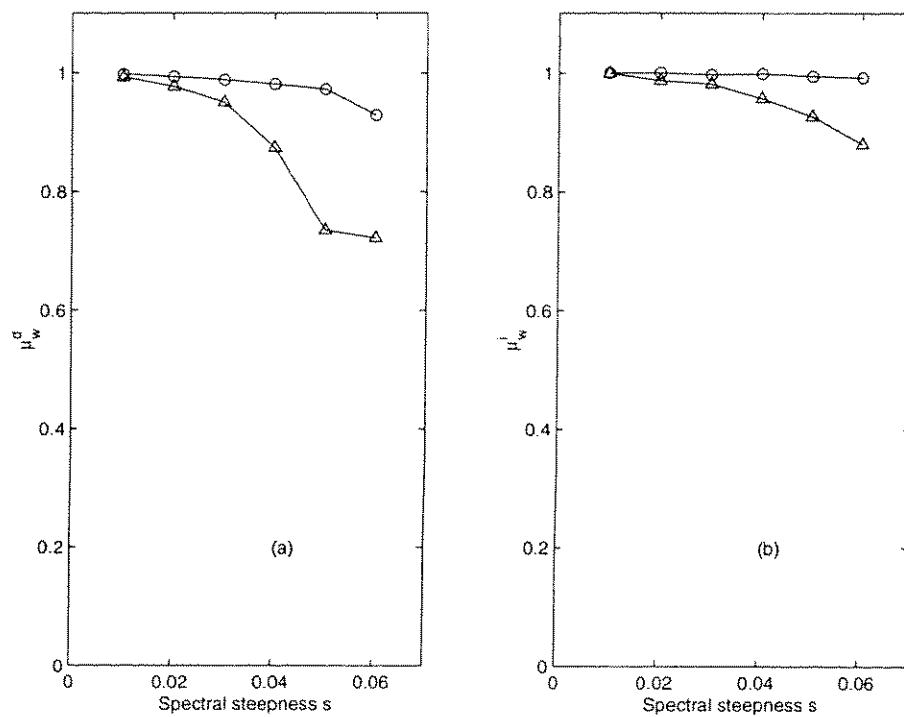


FIGURE 18. μ_w versus s , (a) drag force (b) inertia force; (-o-): Gamma spectrum with $p=9$; (- Δ -): Gamma Spectrum with $p=5$, $\omega_c = 5\omega_p$.

interaction of $p = 5$ spectrum is stronger than that of $p = 9$ for the same spectral steepness.

Wheeler stretching may underestimate the irregular wave kinematics under wave peaks. The underestimate of wave kinematics directly leads to the underestimates of wave forces for relatively steep waves. It is necessary to apply a nonlinear wave model method instead of Wheeler stretching method to estimate the wave forces for steep waves.

CHAPTER V

CONCLUSIONS

A new hybrid wave model (HWM) has been developed. It uses the MCM and PMM solutions to model wave-wave interactions between free-wave components in an ocean field. The MCM solution is derived for wave-wave interaction between free-wave components in directional intermediate-depth water, while the PMM is derived for a deep-water short wave component modulated by intermediate-depth long wave components. The HWM divides a broad-band wave spectrum into several wave bands so that the MCM solution and the PMM are applied to compute the wave-wave interaction accordingly. Nonlinear wave-wave interactions between the same and neighboring bands are computed by the MCM solution while the interactions of wave components that are relatively far apart in the frequency domain are computed by the PMM.

The MCM solution is shown to be identical to the PMM under the condition of $\varepsilon_1 \ll \varepsilon_l < 0.5$. However, under the condition of $\varepsilon_1 > \varepsilon_l$, the MCM solution is divergent while the PMM remains convergent. Therefore it is improper to apply the MCM solution to predict the wave kinematics of a broad-band and strongly nonlinear wave spectrum.

The HWM is applied to compute the wave forces on a SDOF cylindrical structure. Time domain simulation is employed. Truncated Gamma spectra are used for determining the amplitudes of free-wave components. The effects of surface intermittency and wave nonlinearity are studied using the HWM. It is concluded that for this type of structure, the overall effects of surface fluctuation and wave nonlinearity increase with the increase in the spectral steepness. For relatively steep waves, the effects of surface fluctuation and wave nonlinearity may be significant. Both wave

nonlinearity and surface intermittency hence should be considered to estimate the wave forces. Neglecting of either factor may underestimate the wave forces.

It is also concluded that the surface and wave nonlinearity effects also depend on the characteristics of the input wave spectrum. The effects are greater for a spectrum of broader powerful region than that of a narrower one because of the nonlinear interaction is stronger for the broader spectrum than for the narrower one.

Hu et al. (1995) used the MCM to study the wave nonlinearity and surface intermittency effects on fixed slender structures. Their computation considered broad-banded Gamma spectra and used high cutoff frequencies. The computation of wave forces are found to be incorrect due to the divergent wave kinematics resulting from the MCM solution. The sensitivity of wave forces computation depending on the inclusion of trivial amplitude high frequency wave components, was also due to the divergence of the MCM solution. The HWM can render convergent prediction of wave kinematics and hence the predicted wave forces are consistent. As a result they are not sensitive whether or not to the inclusion of trivial amplitude wave components. Based on the simulations, a desirable cutoff frequency of 3 – 5 times of the peak frequency has been proposed for the design practice. It is suggested that the cutoff frequency be chosen in the range of 3 – 5 peak frequency according to the characteristics of the spectrum. For a spectrum with relatively broad powerful bands, a cutoff frequency may be chosen to close the 5 times peak frequency. For a relatively narrow spectrum, a cutoff frequency of $3\omega_p$ is suggested.

The approach for the prediction of irregular wave forces recommended by API (1993) is also compared to compute the wave forces on a SDOF structure with the HWM. It is found that the recommended approach may underestimate the wave forces for relatively steep waves.

The HWM was developed for unidirectional irregular waves by Zhang et al.

(1993). This model was recently developed to allow wave directionality (Zhang et al. 1998). It has been successfully applied to the decomposition and prediction of irregular wave kinematics of both unidirectional and directional irregular waves (Zhang et al. 1996 & 1998). Cao (1996) applied the unidirectional HWM to predict the slow motion of a three DOF spar structure and excellent agreements have been found between the prediction and the experimental data. In this paper, the author used this model to study the nonlinearity of wave kinematics and the surface intermittency and wave nonlinearity effects on wave loads on slender body structures. As the HWM is in its infant stage, still more of its applications need to be discovered in the fields of oceanography, ocean and offshore engineering. For example, wave directionality effects on the structure loads and motion has attracted hydrodynamicists for a long time. It is also very challenging and urgent to combine stochastic analysis tools and the HWM together, which will surely find this robust nonlinear wave model more applications in the ocean science and engineering fields.

REFERENCES

- [1] American Petroleum Institute, API. (1993). Recommended practice for planning, designing and constructing fixed offshore platforms- load and resistance factor design. *API recommended practice 2A-LRFD (RP-LRFD)*, first edition, July 1, 1993.
- [2] Bea, R.G. (1996). Nonlinear performance of offshore platforms in extreme storm waves. *J. Wtrwy., Port, Coast., and Oc. Engrg.*, Vol. 122, No 2, pp. 68–74.
- [3] Borgman, L.E. (1990). Irregular ocean waves: kinematics and forces, in *The Sea*, Vol.9, *Ocean Engineering Science, Part A*, pp. 121–168, J. Wiley, New York.
- [4] Cao, P. (1996). Slow motion responses of compliant offshore structures. *M. Sc. thesis, Texas A&M University, College Station, TX.*
- [5] Chakrabarti, S.K. (1987). *Hydrodynamics of offshore structures*, Computational Mechanics Publications, New York.
- [6] Chen, L., Zhang, J. (1997). On general third-order solutions for irregular waves in deep water. *Ocean Engrg.*, (in press).
- [7] Dean, R. G. (1990). Water wave kinematics: state of the art and future research needs. *Water wave kinematics*, NATO ASI series, series E: Applied sciences, Vol. 178, pp. 743-756.
- [8] Donelan M.A., Anctil, F. and Doering, J.C. (1992). A simple method for calculating the velocity field beneath irregular waves. *Coastal Engrg.*, Vol. 16, pp. 399–424.
- [9] Hallam, M.G., Heaf, N.J. and Wootton, L.R. (1978). *Dynamics of marine structures: methods of calculating the dynamic response of fixed structures subject to wave and current action*, CIRIA Underwater Engineering Group Report UR8.

- [10] Hong K. (1993). Nonlinear interactions between directional dual component waves in deep water. *Ph. D. Thesis, Texas A&M University, College Station, TX.*
- [11] Hsu, J. R. C., Tsuchiya, Y. and Silvester, R. (1979). Third-order approximation to short-crested waves *J. Fluid Mech.*, 90, pp. 179–196.
- [12] Hu, S.J., Zhao, D. (1992). Kinematics of nonlinear random waves near free surface. *J. of Engrg. Mech.*, Vol. 118, No. 10, pp. 2072–2086.
- [13] Hu, S.J., Gupta, M. and Zhao D. (1995). Effects of wave intermittency / nonlinearity on forces and responses. *J. of Engrg. Mech.*, Vol. 121, No. 7, pp. 819–827.
- [14] Huang, N. E., Tung, C. C. and Long, S. R. (1990). Wave spectra. *The sea: ocean engineering science*, Vol. 9, 197–238, John Wiley and Sons, New York.
- [15] Longuet-Higgins, M.S. (1960). Changes in the form of short gravity waves on the long waves and tidal currents. *J. Fluid Mech.*, 8, pp. 565–583.
- [16] Longuet-Higgins, M.S. (1962). Resonant interactions between two trains of gravity waves. *J. Fluid Mech.*, 12, pp. 321–332.
- [17] Longuet-Higgins, M.S. (1963). The effects of non-linearity on statistical distributions in the theory of sea waves. *J. Fluid Mech.*, 17, pp. 459–480.
- [18] Morison, J.R., O'Brien, M.P., Johnson, J.W., and Schaaf, S.A. (1950). The forces exerted by surface waves on piles. *Petroleum Transactions*, 189.
- [19] Pierson, W.J. and Moskowitz, L. (1964). A proposed spectral form for fully developed wind seas based on the similarity theory of S.A. Kitaigorodskii. *J. Geophys. Res.*, Vol 69, pp. 5181–5190.

- [20] Press, W.H., Teukolsky, S.A., Vetterling, W.T., and Flannery, B.P. (1992). *Numerical recipes in FORTRAN: the art of scientific computation*, 2nd edition, Cambridge, New York.
- [21] Prislín, I. (1996). Nonlinear deterministic decomposition of short-crested ocean wave. *Ph. D. Thesis, Texas A&M University, College Station, TX.*
- [22] Prislín, I., Zhang, J. and Seymour, R. J. (1997). Deterministic decomposition of deep water short-crested irregular gravity waves. *J. Geophys. Res.*, 102(C6), pp. 12,677–12,688.
- [23] Sumer, M.B., Fredsoe, J. (1997). Hydrodynamics around cylindrical structures. *Advanced Series on Ocean Engineering*, Vol. 12, pp. 297–330, *World Scientific*, Singapore.
- [24] Sarpkaya, T., Isaacson M. (1981). *Mechanics of wave forces on offshore structures*, Van Nostrand Reinhold Company Inc, New York.
- [25] Spell, C. A., Zhang, J. and Randall, R. E. (1996). Hybrid wave model for unidirectional irregular waves, part II, comparison with laboratory measurements. *J. Applied Ocean Res.*, Vol. 18, pp. 93–110.
- [26] Tayfun, M. A. (1990). High-wave number/frequency attenuation of wind-wave spectrum. *J. Watrwy., Port, Coast., and Oc. Engrg.*, 116(3), pp. 381–398.
- [27] Tung, C.C and Yang, C.H. (1991). Effects of free surface fluctuation on response of offshore structures. *Proc. of 1st Int. Offshore and Polar Engrg. Conf.*, pp. 183–193.
- [28] Wheeler, J.D. (1969). Method of calculating forces produced by irregular waves. *Proc. of First Offshore Tech. Conf.*, OTC 1006, Houston.

- [29] Ye, M. (1994). Predictions of unidirectional irregular wave kinematics and evolution. *M. Sc. Thesis, Texas A&M University, College Station, TX.*
- [30] Zhang, J. and Melville, W.K.(1990). Evolution of weakly nonlinear short waves riding on long gravity waves. *J. Fluid Mech.*, 214, pp. 321-346.
- [31] Zhang, J., Hong, K., and Yue, D.K.P. (1993). Effects of wavelength ratio on wave modeling, *J. Fluid Mech.* 248, pp. 107-127.
- [32] Zhang, J., Chen, L., Ye, M. and Randall, R.E. (1996). Hybrid wave model for unidirectional irregular waves. Part I. Theory and numerical scheme. *J. Appl. Ocean Res.*, 18, pp. 77-92.
- [33] Zhang, J., Conde, E. M. and Seymour, R. J. (1997). Experimental studies on energy dissipation in breaking waves. *Proc. of 7th ISOPE*, Vol. III, pp. 178-183.
- [34] Zhang, J., Conde, E. M. and Yang, J. (1996). Wave elevation based on the pressure measurements. *COE report No. 352, Texas A&M University, College Station, TX.*
- [35] Zhang, J., Yang, J., Wen, J. and Prislun, I. (1998). Deterministic decomposition and prediction of irregular ocean waves. *OTC paper 8660*, (in press).
- [36] Zhang, J., Yang, J., Wen, J. (1998). Directional hybrid wave model and its application. *Waves '98 Proc.*, (in press).
- [37] Zhang, J., Yang, J., Wen, J. and Prislun I. (1998). Deterministic decomposition and prediction of irregular ocean waves. *OTRC report NSF# CDR-8721512.*

APPENDIX A

WAVE PROPERTIES BY THE CONVENTIONAL PERTURBATION SOLUTION

The dynamic pressure head, $z + P/(\rho g)$, can be derived from the Bernoulli equation

$$\frac{\partial \Phi}{\partial t} + \frac{1}{2} |\nabla \Phi|^2 + gz + \frac{P}{\rho} = C_0, \quad (\text{A.1})$$

where ρ is the density of water. For the interaction of two directional wave components, the hydrodynamic pressure obtained by the conventional perturbation solution is,

$$\begin{aligned} z + \frac{P}{\rho g} = & \sum_{i=1}^2 \left\{ a_i K_{pi} \cos \theta_i + \frac{a_i^2 k_i}{2 \sinh(2k_i h)} \{1 - \cosh[2k_i(z+h)]\} \right. \\ & + \frac{a_i^2 k_i}{2 \sinh(2k_i h)} [3(\alpha_i^2 - 1) \cosh 2k_i(z+h) - 1] \cos 2\theta_i \} \\ & + \frac{a_1 a_2 k_2}{2\alpha_2} \left[-(1-\lambda) A_{(-)} \frac{\cosh[|\mathbf{k}_1 - \mathbf{k}_2|(z+h)]}{\cosh(|\mathbf{k}_1 - \mathbf{k}_2|h)} + E_{(-)} \right] \cos(\theta_1 - \theta_2) \\ & + \frac{a_1 a_2 k_2}{2\alpha_2} \left[(1+\lambda) A_{(+)} \frac{\cosh[|\mathbf{k}_1 + \mathbf{k}_2|(z+h)]}{\cosh(|\mathbf{k}_1 + \mathbf{k}_2|h)} + E_{(+)} \right] \cos(\theta_1 + \theta_2), \quad (\text{A.2}) \end{aligned}$$

where

$$E_{(\mp)} = -\alpha_1 \alpha_2 \lambda (\Gamma K_{p1} K_{p2} \pm R), \quad (\text{A.3a})$$

$$K_{pi} = \frac{\cosh[k_i(z+h)]}{\cosh k_i h}, \quad i = 1, 2, \quad (\text{A.3b})$$

$$R = \frac{\sinh[k_1(z+h)] \sinh[k_2(z+h)]}{\cosh k_1 h \cosh k_2 h}. \quad (\text{A.3c})$$

where Γ, α_i and λ are defined in Section 2.11.

The velocity components are the spatial derivatives of the potential Φ ,

$$\begin{aligned} u = & \sum_{i=1}^2 \left\{ \frac{a_i g k_{ix}}{\sigma_i} K_{pi} \cos \theta_i + \frac{3 a_i^2 k_{ix} \sigma_i \cosh[2k_i(z+h)]}{4 \sinh^4(k_i h)} \cos(2\theta_i) \right\} \\ & + \frac{a_1 a_2 \sigma_2}{2} A_{(-)} (k_{1x} - k_{2x}) \frac{\cosh[|\mathbf{k}_1 - \mathbf{k}_2|(z+h)]}{\cosh(|\mathbf{k}_1 - \mathbf{k}_2|h)} \cos(\theta_1 - \theta_2) \end{aligned}$$

$$+ \frac{a_1 a_2 \sigma_2}{2} A_{(+)}(k_{1x} + k_{2x}) \frac{\cosh[|\mathbf{k}_1 + \mathbf{k}_2|(z+h)]}{\cosh(|\mathbf{k}_1 + \mathbf{k}_2|h)} \cos(\theta_1 + \theta_2), \quad (\text{A.4a})$$

$$v = \sum_{i=1}^2 \left\{ \frac{a_i g k_{iy}}{\sigma_i} K_{pi} \cos \theta_i + \frac{3 a_i^2 k_{iy} \sigma_i \cosh[2k_i(z+h)]}{4 \sinh^4(k_i h)} \cos(2\theta_i) \right\} \\ + \frac{a_1 a_2 \sigma_2}{2} A_{(-)}(k_{1y} - k_{2y}) \frac{\cosh[|\mathbf{k}_1 - \mathbf{k}_2|(z+h)]}{\cosh(|\mathbf{k}_1 - \mathbf{k}_2|h)} \cos(\theta_1 - \theta_2) \\ + \frac{a_1 a_2 \sigma_2}{2} A_{(+)}(k_{1y} + k_{2y}) \frac{\cosh[|\mathbf{k}_1 + \mathbf{k}_2|(z+h)]}{\cosh(|\mathbf{k}_1 + \mathbf{k}_2|h)} \cos(\theta_1 + \theta_2), \quad (\text{A.4b})$$

$$w = \sum_{i=1}^2 \left\{ \frac{a_i g k_i \sinh[k_i(z+h)]}{\sigma_i \cosh(k_i h)} \sin \theta_i + \frac{3 a_i^2 k_i \sigma_i \sinh[2k_i(z+h)]}{4 \sinh^4(k_i h)} \sin(2\theta_i) \right\} \\ + \frac{a_1 a_2 \sigma_2}{2} A_{(-)} |\mathbf{k}_1 - \mathbf{k}_2| \frac{\sinh[|\mathbf{k}_1 - \mathbf{k}_2|(z+h)]}{\cosh(|\mathbf{k}_1 - \mathbf{k}_2|h)} \sin(\theta_1 - \theta_2) \\ + \frac{a_1 a_2 \sigma_2}{2} A_{(+)} |\mathbf{k}_1 + \mathbf{k}_2| \frac{\sinh[|\mathbf{k}_1 + \mathbf{k}_2|(z+h)]}{\cosh(|\mathbf{k}_1 + \mathbf{k}_2|h)} \sin(\theta_1 + \theta_2). \quad (\text{A.4c})$$

The acceleration includes two parts : local accerelation and convective acceleration.

$$a_x = \sum_{i=1}^2 \left\{ a_i g k_{ix} \frac{\cosh[k_i(z+h)]}{\cosh(k_i h)} \sin \theta_i \right. \\ + \frac{a_i^2 k_{ix} \sigma_i^2}{2 \sinh^2(k_i h)} [3(\alpha_i^2 - 1) \cosh 2k_i(z+h) - 1] \sin(2\theta_i) \left. \right\} \\ \mp \frac{a_1 a_2 (k_{1x} \mp k_{2x}) \sigma_2^2}{2} \left\{ A_{(\mp)} (1 \mp \lambda) \frac{\cosh[|\mathbf{k}_1 \mp \mathbf{k}_2|(z+h)]}{\cosh(|\mathbf{k}_1 \mp \mathbf{k}_2|h)} \pm T_{(\mp)} \right\} \\ \sin(\theta_1 \mp \theta_2), \quad (\text{A.5a})$$

$$a_y = \sum_{i=1}^2 \left\{ a_i g k_{iy} \frac{\cosh[k_i(z+h)]}{\cosh(k_i h)} \sin \theta_i \right. \\ + \frac{a_i^2 k_{iy} \sigma_i^2}{2 \sinh^2(k_i h)} [3(\alpha_i^2 - 1) \cosh 2k_i(z+h) - 1] \sin(2\theta_i) \left. \right\} \\ \mp \frac{a_1 a_2 (k_{1y} \mp k_{2y}) \sigma_2^2}{2} \left\{ A_{(\mp)} (1 \mp \lambda) \frac{\cosh[|\mathbf{k}_1 \mp \mathbf{k}_2|(z+h)]}{\cosh(|\mathbf{k}_1 \mp \mathbf{k}_2|h)} \pm T_{(\mp)} \right\} \\ \sin(\theta_1 \mp \theta_2), \quad (\text{A.5b})$$

$$a_z = \sum_{i=1}^2 \left\{ -a_i g k_i \frac{\sinh[k_i(z+h)]}{\cosh(k_i h)} \cos \theta_i \right. \\ + \frac{a_i^2 k_i \sigma_i^2 \sinh 2k_i(z+h)}{2 \sinh^2(k_i h)} [1 - 3(\alpha_i^2 - 1) \cos 2\theta_i] \left. \right\} \\ + \frac{a_1 a_2 \sigma_2^2}{2} \left\{ A_{(\mp)} |\mathbf{k}_1 \mp \mathbf{k}_2| (1 \mp \lambda) \frac{\sinh[|\mathbf{k}_1 \mp \mathbf{k}_2|(z+h)]}{\cosh(|\mathbf{k}_1 \mp \mathbf{k}_2|h)} + V_{(\mp)} \right\} \\ \cos(\theta_1 \mp \theta_2), \quad (\text{A.5c})$$

where

$$T_{(\mp)} = \frac{\lambda}{\sinh k_1 h \sinh k_2 h} [\Gamma \cosh k_1(z+h) \cosh k_2(z+h) \pm \sinh k_1(z+h) \sinh k_2(z+h)], \quad (\text{A.6a})$$

$$V_{(\mp)} = \frac{\lambda}{\sinh k_1 h \sinh k_2 h} [(\Gamma k_1 \mp k_2) \sinh k_1(z+h) \cosh k_2(z+h) \mp (k_1 \mp \Gamma k_2) \cosh k_1(z+h) \sinh k_2(z+h)]. \quad (\text{A.6b})$$

All of the above formulations of the wave properties by the conventional perturbation solution can be readily extended to that for the interactions of multi-directional wave components by summing over all the wave components.

APPENDIX B

SOLUTION OF MODULATION PARAMETERS

The parameters of phase modulation approach can be obtained from Laplace equation and boundary conditions as shown in Chapter 2. In this study, we truncate the summation at $J = 2$. Therefore the summations of $k_1 z$ polynomials are truncated at ρ_2 and γ_2 respectively. The single summations of τ and b are truncated at τ_3 and b_3 correspondingly. For the summations of ρ_j and γ_j , we will truncate at corresponding λ order according the truncation discussion in Chapter 2. The parameters are listed below. ρ_0 vector is given as:

$$\rho_{00} = \alpha_1 \Gamma \quad (\text{C.1a})$$

$$\rho_{01} = \frac{1}{2}(\alpha_1^2 \Gamma^2 - 1) \quad (\text{C.1b})$$

$$\rho_{02} = \frac{\alpha_1 \Gamma}{4}(\alpha_1^2 \Gamma^2 - 1) \quad (\text{C.1c})$$

$$\rho_{03} = \frac{1}{8}(\alpha_1^4 \Gamma^4 + 2\alpha_1^2 \Gamma^2 - 4\alpha_1^2 + 1) \quad (\text{C.1d})$$

$$\rho_{04} = \frac{\alpha_1 \Gamma}{16}(\alpha_1^4 \Gamma^4 - 2\alpha_1^2 \Gamma^2 + 1) \quad (\text{C.1e})$$

To get a consistant truncation accuracy, we compute the summation of ρ_1 up to ρ_{12} .

$$\rho_{10} = -\Gamma \quad (\text{C.2a})$$

$$\rho_{11} = 0 \quad (\text{C.2b})$$

$$\rho_{12} = \frac{1}{4}(4\alpha_1^2 \Gamma - 3\alpha_1^2 \Gamma^3 - \Gamma) \quad (\text{C.2c})$$

For the summation of ρ_2 , we only compute ρ_{20} term.

$$\rho_{20} = \frac{\alpha_1}{2} \Gamma^3 \quad (\text{C.3})$$

The parametrs γ_0 , γ_1 and γ_2 are listed below. The summation of γ_0 is computed up

to γ_{04} .

$$\gamma_{00} = \alpha_1 \Gamma^2 \quad (\text{C.4a})$$

$$\gamma_{01} = \frac{\Gamma}{2}(\alpha_1^2 \Gamma^2 - 1) \quad (\text{C.4b})$$

$$\gamma_{02} = \frac{\alpha_1}{4}(\alpha_1^2 \Gamma^4 + \Gamma^2 - 2) \quad (\text{C.4c})$$

$$\gamma_{03} = \frac{\Gamma}{8}(\alpha_1^4 \Gamma^4 + 2\alpha_1^2 \Gamma^2 - 4\alpha_1^2 + 1) \quad (\text{C.4d})$$

$$\gamma_{04} = \frac{\alpha_1}{16}(\alpha_1^4 \Gamma^6 + 8\alpha_1^2 \Gamma^4 + 3\Gamma^2 - 14\alpha_1^2 \Gamma^2 + 4\alpha_1^2 - 2) \quad (\text{C.4e})$$

The summation of γ_1 is computed up to γ_{12} .

$$\gamma_{10} = -\frac{1}{2}\Gamma^2 \quad (\text{C.5a})$$

$$\gamma_{11} = 0 \quad (\text{C.5b})$$

$$\gamma_{12} = \frac{\Gamma^2}{8}(6\alpha_1^2 - 5\alpha_1 \Gamma^2 - 1) \quad (\text{C.5c})$$

Only γ_{20} is considered for the summation of γ_2 .

$$\gamma_{20} = \frac{\alpha_1}{6}\Gamma^4 \quad (\text{C.6})$$

For the parameter of τ , we truncate the summation at τ_3 .

$$\tau_0 = \frac{1}{4}(2\alpha_1 - \alpha_1 \Gamma^2 - \alpha_1^{-1}) \quad (\text{C.7a})$$

$$\tau_1 = \frac{1}{2}\alpha_1^2 \Gamma(1 - \Gamma^2) \quad (\text{C.7b})$$

$$\tau_2 = \frac{1}{16}[2\alpha_1 - \alpha_1^{-1} - \alpha_1^3(5\Gamma^4 + 2\Gamma^3 - 6\Gamma^2)] \quad (\text{C.7c})$$

$$\tau_3 = \frac{1}{16}(-4\alpha_1^4 \Gamma^5 - \alpha_1^4 \Gamma^4 + 4\alpha_1^4 \Gamma^3 - 6\alpha_1^2 \Gamma^3 + 12\alpha_1^2 \Gamma - \Gamma) \quad (\text{C.7d})$$

Once τ is obtained, the phase modulation parameter of surface elevation Δ can be computed.

$$\Delta = \lambda \tau \quad (\text{C.8})$$

The summation of b is truncated at b_3 .

$$b_0 = \frac{2\alpha_1 + \alpha_1\Gamma^2 + \alpha_1^{-1}}{4} \quad (\text{C.9a})$$

$$b_1 = \frac{\Gamma(2\alpha_1^2 - \alpha_1^2\Gamma^2 - 1)}{4} \quad (\text{C.9b})$$

$$b_2 = \frac{\alpha_1^{-1} - \alpha_1(6 - 4\Gamma^2) + \alpha_1^3\Gamma^2(6 - 3\Gamma^2 - 2\Gamma)}{16} \quad (\text{C.9c})$$

$$b_3 = \frac{1}{16}(\alpha_1^5\Gamma^5 + 4\alpha_1^4\Gamma^5 + \alpha_1^4\Gamma^4 - 4\alpha_1^4\Gamma^3 - 2\alpha_1^3\Gamma^3 + 6\alpha_1^2\Gamma^3 - 12\alpha_1^2\Gamma + \alpha_1\Gamma + \Gamma) \quad (\text{C.9d})$$

APPENDIX C

WAVE PROPERTIES BY THE PHASE MODULATION SOLUTION

The dynamic pressure of the modulated short wave component by a long wave component can be obtained from the Bernoulli equation

$$\frac{P_3}{\rho g} + z = -\frac{1}{g} \nabla \Phi_3 \cdot \nabla \Phi_1 - \frac{1}{g} \frac{\partial \Phi_3}{\partial t} - \frac{1}{2g} |\nabla \Phi_3|^2, \quad (\text{C.1})$$

with

$$\Phi_1 = \frac{a_1 g \cosh[k_1(z+h)]}{\sigma_1 \cosh(k_1 h)} \sin \theta_1, \quad (\text{C.2})$$

where the subscripts 1 and 3 represent the long wave component and the modulated short wave component, respectively. Hence, by substituting the phase modulation solution given in § 2.1.2 into Equation (C.1), we have

$$\frac{P_3}{\rho g} + z = a_3 e^{k_3 f k} \left[(1 + \varepsilon_1 C \cos \theta_1) \cos \tilde{\theta}_3 + \varepsilon_1 S \sin \theta_1 \sin \tilde{\theta}_3 \right], \quad (\text{C.3})$$

where

$$C = \tau - \lambda^{-1} \Gamma K_{p1} + \lambda^{-1} \alpha_1^{-1} \sum_{j=0}^{J+1} \rho_j (k_1 z)^j, \quad (\text{C.4a})$$

$$S = -\tau \lambda + \lambda^{-1} \alpha_1^{-1} - \lambda^{-1} H_{p1} - \lambda k_3 z \sum_{j=0}^{J+1} \gamma_j (k_1 z)^j, \quad (\text{C.4b})$$

$$H_{p1} = \frac{\sinh[k_1(z+h)]}{\cosh k_1 h}, \quad (\text{C.4c})$$

where Γ, K_{p1} were defined in Equation (2.6d) and (A.3b) respectively.

The velocity components of the modulated short wave component can be calculated by the spatial derivatives of Φ_3 ,

$$u = a_3 \sigma_3 e^{k_3 f k} [(\cos \beta_3 + \varepsilon_1 C_u \cos \theta_1) \cos \tilde{\theta}_3 + \varepsilon_1 S_u \sin \theta_1 \sin \tilde{\theta}_3], \quad (\text{C.5a})$$

$$v = a_3 \sigma_3 e^{k_3 f k} [(\sin \beta_3 + \varepsilon_1 C_v \cos \theta_1) \cos \tilde{\theta}_3 + \varepsilon_1 S_v \sin \theta_1 \sin \tilde{\theta}_3], \quad (\text{C.5b})$$

$$w = a_3 \sigma_3 e^{k_3 f_k} [\varepsilon_1 C_w \sin \theta_1 \cos \tilde{\theta}_3 + (1 + \varepsilon_1 S_w \cos \theta_1) \sin \tilde{\theta}_3], \quad (\text{C.5c})$$

where

$$C_u = \tau \cos \beta_3 + \cos \beta_1 \sum_{j=0}^{J+1} \rho_j (k_1 z)^j, \quad (\text{C.6a})$$

$$C_v = \tau \sin \beta_3 + \sin \beta_1 \sum_{j=0}^{J+1} \rho_j (k_1 z)^j, \quad (\text{C.6b})$$

$$C_w = \sum_{j=1}^{J+1} j \rho_j (k_1 z)^{j-1}, \quad (\text{C.6c})$$

$$S_u = \cos \beta_1 \left[1 - \tau \lambda^2 \alpha_1 - \sum_{j=0}^{J+1} \gamma_j (k_1 z)^{j+1} \right], \quad (\text{C.6d})$$

$$S_v = \sin \beta_1 \left[1 - \tau \lambda^2 \alpha_1 - \sum_{j=0}^{J+1} \gamma_j (k_1 z)^{j+1} \right], \quad (\text{C.6e})$$

$$S_w = \tau + \sum_{j=0}^{J+1} (j+1) \gamma_j (k_1 z)^j. \quad (\text{C.6f})$$

The acceleration of the modulated short wave component is in the form of

$$\mathbf{a} = \left\{ \begin{array}{l} \frac{\partial u_3}{\partial t} + (u_1 + u_3) \frac{\partial u_3}{\partial x} + (v_1 + v_3) \frac{\partial u_3}{\partial y} + (w_1 + w_3) \frac{\partial u_3}{\partial z} \\ \frac{\partial v_3}{\partial t} + (u_1 + u_3) \frac{\partial v_3}{\partial x} + (v_1 + v_3) \frac{\partial v_3}{\partial y} + (w_1 + w_3) \frac{\partial v_3}{\partial z} \\ \frac{\partial w_3}{\partial t} + (u_1 + u_3) \frac{\partial w_3}{\partial x} + (v_1 + v_3) \frac{\partial w_3}{\partial y} + (w_1 + w_3) \frac{\partial w_3}{\partial z} \end{array} \right\}, \quad (\text{C.7})$$

where the first-order long wave velocity components are,

$$u_1 = \frac{a_1 g k_1}{\sigma_1} K_{p1} \cos \beta_1 \cos \theta_1, \quad (\text{C.8a})$$

$$v_1 = \frac{a_1 g k_1}{\sigma_1} K_{p1} \sin \beta_1 \cos \theta_1, \quad (\text{C.8b})$$

$$w_1 = \frac{a_1 g k_1}{\sigma_1} H_{p1} \sin \theta_1, \quad (\text{C.8c})$$

the time derivatives of the modulated velocity components are

$$\begin{aligned} \frac{\partial_3}{\partial t} = & a_3 \sigma_3^2 e^{k_3 f_k} \left\{ \sin \tilde{\theta}_3 [\cos \beta_3 + a_1 k_3 \lambda \cos \theta_1 \cos \beta_3 \sum_{j=0}^{J+1} \rho_j (k_1 z)^j + \varepsilon_1 C_u \cos \theta_1 \right. \\ & \left. - \varepsilon_1 \lambda S_u \cos \theta_1] + \cos \tilde{\theta}_3 \sin \theta_1 [\lambda \varepsilon_1 C_u - \varepsilon_1 S_u - a_1 k_3 \lambda \cos \beta_3 \right. \end{aligned}$$

$$+\varepsilon_1 \lambda k_3 z \cos \beta_3 \sum_{j=0}^{J+1} \gamma_j (k_1 z)^{j+1} \}, \quad (\text{C.9a})$$

$$\begin{aligned} \frac{\partial v_3}{\partial t} = & a_3 \sigma_3^2 e^{k_3 f_k} \{ \sin \bar{\theta}_3 [\sin \beta_3 + a_1 k_3 \lambda \cos \theta_1 \sin \beta_3 \sum_{j=0}^{J+1} \rho_j (k_1 z)^j + \varepsilon_1 C_v \cos \theta_1 \\ & - \varepsilon_1 \lambda S_v \cos \theta_1] + \cos \bar{\theta}_3 \sin \theta_1 [\varepsilon_1 \lambda C_v - \varepsilon_1 S_v - a_1 k_3 \lambda \sin \beta_3 \\ & + \varepsilon_1 \lambda k_3 z \sin \beta_3 \sum_{j=0}^{J+1} \gamma_j (k_1 z)^{j+1}] \}, \end{aligned} \quad (\text{C.9b})$$

$$\begin{aligned} \frac{\partial w_3}{\partial t} = & a_3 \sigma_3^2 e^{k_3 f_k} \{ \sin \bar{\theta}_3 \sin \theta_1 [\varepsilon_1 \lambda S_w - a_1 k_3 \lambda + \varepsilon_1 \lambda k_3 z \sum_{j=0}^{J+1} \rho_j (k_1 z)^j + \varepsilon_1 C_w] \\ & + \cos \bar{\theta}_3 [-1 - \varepsilon_1 \lambda \cos \theta_1 - \varepsilon_1 S_w \cos \theta_1 - a_1 k_3 \lambda \sum_{j=0}^{J+1} \rho_j (k_1 z)^j] \} \end{aligned} \quad (\text{C.9c})$$

and the spatial derivatives of the modulated velocity components are:

$$\frac{\partial u_3}{\partial x} = -a_3 \sigma_3 k_3 e^{k_3 f_k} \cos^2 \beta_3 \sin \bar{\theta}_3, \quad (\text{C.10a})$$

$$\frac{\partial u_3}{\partial y} = -a_3 \sigma_3 k_3 e^{k_3 f_k} \cos \beta_3 \sin \beta_3 \sin \bar{\theta}_3, \quad (\text{C.10b})$$

$$\frac{\partial u_3}{\partial z} = a_3 \sigma_3 k_3 e^{k_3 f_k} \cos \beta_3 \cos \bar{\theta}_3, \quad (\text{C.10c})$$

$$\frac{\partial v_3}{\partial x} = \frac{\partial u_3}{\partial y}, \quad (\text{C.10d})$$

$$\frac{\partial v_3}{\partial y} = -a_3 \sigma_3 k_3 e^{k_3 f_k} \sin^2 \beta_3 \sin \bar{\theta}_3, \quad (\text{C.10e})$$

$$\frac{\partial v_3}{\partial z} = a_3 \sigma_3 k_3 e^{k_3 f_k} \sin \beta_3 \cos \bar{\theta}_3, \quad (\text{C.10f})$$

$$\frac{\partial w_3}{\partial x} = \frac{\partial u_3}{\partial z}, \quad (\text{C.10g})$$

$$\frac{\partial w_3}{\partial y} = \frac{\partial v_3}{\partial z}, \quad (\text{C.10h})$$

$$\frac{\partial w_3}{\partial z} = a_3 \sigma_3 k_3 e^{k_3 f_k} \sin \bar{\theta}_3. \quad (\text{C.10i})$$

For a short wave modulated by M long wave components, the modulated surface elevation is the sum of the modulations by all M long wave components,

$$\eta_3 = a_3 \left(1 + \sum_{m=1}^M \varepsilon_m b_m \cos \theta_m \right) \cos(\bar{\theta}_3), \quad (\text{C.11})$$

where

$$\tilde{\theta}_3 = k_{3x}x + k_{3y}y - \sigma_3 t + \delta_3 + \sum_{m=1}^M k_3 a_m \rho_{0m} \sin \theta_m + \sum_{m=1}^M \Delta_m \varepsilon_m \sin \theta_m, \quad (\text{C.12a})$$

$$\Delta_m = \lambda_m \tau_m, \quad \lambda_m = \frac{\sigma_m}{\sigma_3}. \quad (\text{C.12b})$$

The modulated dynamic pressure is, then,

$$\frac{P_3}{\rho g} + z = a_3 e^{k_3 f_k} \left[(1 + \varepsilon_1 C \cos \theta_1) \cos \tilde{\theta}_3 + \varepsilon_1 S \sin \theta_1 \sin \tilde{\theta}_3 \right], \quad (\text{C.13})$$

with

$$C = \sum_{m=1}^M \left[\tau_m - \lambda_m^{-1} \Gamma_m K_{pm} + \lambda_m^{-1} \alpha_m^{-1} \sum_{j=0}^{J+1} \rho_{mj} (k_m z)^j \right], \quad (\text{C.14a})$$

$$S = \sum_{m=1}^M \left[-\tau_m \lambda_m + \lambda_m^{-1} \alpha_m^{-1} - \lambda_m^{-1} H_{pm} - \lambda_m k_3 z \sum_{j=0}^{J+1} \gamma_{mj} (k_m z)^j \right], \quad (\text{C.14b})$$

$$\lambda_m = \frac{\sigma_m}{\sigma_3}, \quad H_{pm} = \frac{\sinh[k_m(z+h)]}{\cosh k_m h}, \quad K_{pm} = \frac{\cosh[k_m(z+h)]}{\cosh k_m h}. \quad (\text{C.14c})$$

The modulated velocity components are in the same form as (C.5), but with

$$C_u = \sum_{m=1}^M \left[\tau_m \cos \beta_3 + \cos \beta_m \sum_{j=0}^{J+1} \rho_{mj} (k_m z)^j \right], \quad (\text{C.15a})$$

$$C_v = \sum_{m=1}^M \left[\tau_m \sin \beta_3 + \sin \beta_m \sum_{j=0}^{J+1} \rho_{mj} (k_m z)^j \right], \quad (\text{C.15b})$$

$$C_w = \sum_{m=1}^M \sum_{j=1}^{J+1} j \rho_{mj} (k_m z)^{j-1}, \quad (\text{C.15c})$$

$$S_u = \sum_{m=1}^M \cos \beta_m \left[1 - \tau_m \lambda_m^2 \alpha_m - \sum_{j=0}^{J+1} \gamma_{mj} (k_m z)^{j+1} \right], \quad (\text{C.15d})$$

$$S_v = \sum_{m=1}^M \sin \beta_m \left[1 - \tau_m \lambda_m^2 \alpha_m - \sum_{j=0}^{J+1} \gamma_{mj} (k_m z)^{j+1} \right], \quad (\text{C.15e})$$

$$S_w = \sum_{m=1}^M \left[\tau_m + \sum_{j=0}^{J+1} (j+1) \gamma_{mj} (k_m z)^j \right]. \quad (\text{C.15f})$$

The modulated acceleration components can be calculated as (C.7), but with the summation over all the long wave components,

$$u_1^{(1)} = \sum_{m=1}^M \frac{a_m g k_m}{\sigma_m} K_{pm} \cos \beta_m \cos \theta_m, \quad (\text{C.16a})$$

$$v_1^{(1)} = \sum_{m=1}^M \frac{a_m g k_m}{\sigma_m} K_{pm} \sin \beta_m \cos \theta_m, \quad (\text{C.16b})$$

$$w_1^{(1)} = \sum_{m=1}^M \frac{a_m g k_m}{\sigma_m} H_{pm} \sin \theta_m, \quad (\text{C.16c})$$

$$f_k = z - \sum_{m=1}^M \left\{ a_m \cos \theta_m + \varepsilon_m z \cos \theta_m \left[\sum_{j=0}^J \gamma_{jm} (k_m z)^j \right] \right\}, \quad (\text{C.16d})$$

$$\tilde{\theta}_3 = k_{3x} x + k_{3y} y - \sigma_3 t + \delta_3 + \sum_{m=1}^M \left[k_3 a_m \sin \theta_m \sum_{j=0}^J \rho_{jm} (k_m z)^j \right]. \quad (\text{C.16e})$$

APPENDIX D

NOMENCLATURE

The following symbols are used in this thesis.

a	wave amplitude
(a_x, a_y, a_z)	total acceleration vector
B, C, p, q	Gamma spectrum parameter
C_0	Bernoulli constant
C_D	drag coefficient
C_M	inertia coefficient
ω_p	peak wave frequency
ω_c	cut off frequency
$\rho, \gamma, \tau, \Delta, b$	Phase modulation parameters
Φ	velocity potential
K_p	$\frac{\cosh[k(z+h)]}{\cosh kh}$
Γ	$\cos(\beta_1 - \beta_2)$
H_{p1}	$\frac{\sinh[k_1(z+h)]}{\sinh k_1 h}$
P	pressure head
f_A, f_k	modulation parameters
$\tilde{\theta}_3$	modulated phase for potential
$\tilde{\theta}_3$	modulation phase of elevation
R	$\frac{\sinh[k_1(z+h)] \sinh[k_2(z+h)]}{\cosh k_1 h \cosh k_2 h}$
h	water depth
g	gravity acceleration
S_{η_1}, S_{η}	resultant and free-wave spectral density function, respectively

ω	wave radian frequency
\mathbf{k}	wave number vector
t	time
(x,y,z)	Cartesian coordinates
z	vertical position
ε_1	long wave steepness
ε_l	wave length ratio of short to long wave
ϵ	spectral bandwidth parameter
s	spectral steepness
λ	frequency ratio of short to long
θ	linear wave phase
η_1, η_2	first- and second-order surface elevation, respectively
(u,v,w)	velocity vector
β	wave propagation angles
δ	initial phases
σ_η	standard deviation of surface elevation
σ^d, σ^i	standard deviations of drag and inertia wave forces
μ_1, μ_2, μ_3	ratios of wave forces standard deviations (three different methods)
μ_c	ratios of wave forces standard deviations for different cut off frequencies
μ_w	ratios of wave forces standard deviations of Wheeler to HWM